

Rearrangements in model face-centered-cubic solids

David J. Wales and Julia Uppenbrink*

University Chemical Laboratories, Lensfield Road, Cambridge CB2 1EW, United Kingdom

(Received 9 June 1994; revised manuscript received 2 August 1994)

Minima, transition states, and rearrangement pathways have been calculated by eigenvector following for model face-centered-cubic solids. Results are reported for systems bound by three empirical potentials representing Au, Ag, and C₆₀. Various vacancy and interstitial diffusion processes are investigated, and diffusion constants, formation energies, and migration energies are compared between the different systems. In addition to these generally localized mechanisms, several highly cooperative rearrangements were found, and the possible significance of these results, and of the effects of lattice relaxation, is discussed.

I. INTRODUCTION

Finding atomic configurations which correspond to local energy minima is usually not difficult given a model for the energy as a function of the coordinates. To discuss dynamics, however, one needs to characterize transition states, which correspond to structures of highest energy on lowest-energy pathways between pairs of minima. In recent years considerable progress has been made in finding transition states and rearrangement mechanisms in progressively larger systems. The purpose of this paper is to show how such methods can be applied to extended systems with periodic boundary conditions representing bulk material or surfaces.

The results presented in this paper are all for face-centered-cubic systems and employ empirical potentials. The solids in question are Ag and Au, represented by different forms of a many-body potential due to Sutton and Chen¹ (SC), and C₆₀, represented by an intermolecular potential due to Girifalco.² The functional forms are given in Sec. III and the optimization method used to locate all the minima and transition states and characterize the rearrangement pathways is described in Sec. IV. A number of vacancy (Sec. VI) and interstitial (Sec. VII) migration mechanisms are identified, giving formation and migration energies, as well as diffusion constants (Sec. IX). Some highly cooperative processes are described in Sec. VIII. It is also important to consider the differences between calculations performed at constant volume and at constant pressure, i.e., where the lattice is allowed to relax. Results are given in Sec. IX where it is shown that relaxation does not affect the energetics significantly, but can have dramatic consequences for the diffusion constants. Conclusions are presented in Sec. X.

II. DEFECTS AND DIFFUSION

It is generally accepted, following Huntingdon and Seitz,³ that nearest-neighbor vacancy migration is the most energetically favorable defect diffusion mechanism in metals. However, there has been some debate about the cause of the upward curvature of Arrhenius plots, i.e., the logarithm of the diffusion constant as a function

of the reciprocal temperature. This effect is especially pronounced in the group-4 body-centered-cubic metals β -Ti, β -Zr, and β -Hf, and phonon interactions combined with a temperature-dependent vacancy migration enthalpy may be responsible.⁴ The energy barrier to migration calculated from simulations by Mikhin and Osetsky⁴ was smaller than for a static calculation, and it was suggested that this is due to the presence of a "dynamic double barrier."⁵ Here, however, we will concentrate on the potential-energy surface.

For the refractory body-centered-cubic metals of groups 5 and 6 the Arrhenius plot curvature is less pronounced, and Neumann *et al.* concluded that two diffusion mechanisms are responsible.⁶ They further argued that a divacancy contribution can be neglected, and that a second-nearest-neighbor process is more likely to provide the additional mechanism than rearrangements involving interstitial atoms. The presence of two different kinds of interstitial defects in the group-4 metals, and perhaps groups 5 and 6 as well, has been suggested by Frank.⁷

For face-centered-cubic metals the enhanced rate of diffusion at high temperatures is qualitatively similar to that observed for the group-5 and -6 metals. Siegel⁸ pointed out that this could be due to temperature-dependent properties of the monovacancies or, more likely, contributions from other mechanisms at higher temperatures. For Al, Au, and Pt he argued that divacancies are the second mechanism in question, but that interstitials could also be involved in other face-centered-cubic metals. Schüle⁹ described the divacancy contribution to diffusion in Au as "especially small" and "relatively large in Cu and Ag, even below 700°C," and also ruled out a significant temperature dependence of both monovacancy and divacancy parameters, with the possible exception of Ag. However, the small contribution of the divacancy mechanism in Au is all that is needed to explain the very small curvature exhibited for this metal.⁹ In contrast, Fuks *et al.* interpreted their calculations for face-centered-cubic Cs in terms of the variation of the energy of vacancy formation with the concentration of vacancies.¹⁰

III. POTENTIALS AND CALCULATION OF THE ENERGY

The present study employs empirical potentials for Ag, Au, and C₆₀, both to provide benchmark calculations for these systems and because accurate quantum-mechanical descriptions would be very time consuming. We do not expect these forms to give high accuracy, although previous results for Sutton-Chen potentials are encouraging. Since only equilibrium data have been used in the parametrizations we should not expect quantities such as barrier heights to be as accurate as vacancy formation energies. However, the main purpose of the present paper is to demonstrate that eigenvector following can reveal rearrangement mechanisms and activation barriers in model bulk systems if energy derivatives are available. Although the whole concept of a transition state can be avoided using a quantum-mechanical approach,¹¹ most previous considerations of rate processes are essentially classical, following Vineyard,¹² and this framework will also be used in the present work.

The Sutton-Chen¹ form used for Ag and Au is an extension of the many-body approach developed by Finnis and Sinclair¹³ intended to give a realistic description of long-range as well as short-range interactions in transition metals. The need to extend empirical descriptions of metals beyond a simple pair representation has been recognized for some time, and various approaches have been suggested, starting from the inclusion of three-body terms.^{14,15} Both the Finnis-Sinclair and embedded-atom¹⁶ models represent the cohesive energy by an attractive functional of the electron density and a repulsive pair potential. Physically reasonable inward surface relaxations have been obtained with such potentials.¹⁷ The Sutton-Chen form has also been found to give results in agreement with experiment in describing the migration of surface atoms¹⁸ and surface relaxation.¹⁵ The structural and dynamical implications of such potentials for clusters have also been investigated.¹⁹ The energy in this approach is written as

$$V_{SC} = \epsilon \left[\sum_{i < j} \left(\frac{a}{r_{ij}} \right)^n - c \sum_i \sqrt{\rho_i} \right],$$

where

$$\rho_i = \sum_{j \neq i} \left(\frac{a}{r_{ij}} \right)^m \quad (1)$$

is the local "density" at atom i , r_{ij} is the separation of atoms i and j , ϵ is a parameter with dimensions of energy, a is a parameter with dimensions of length, c is a dimensionless parameter, and the exponents n and m are constrained to be integers.¹ The fitted values recommended by Sutton and Chen are $\epsilon = 0.0025415$ eV, $a = 4.09$ Å, $c = 144.41$, $n = 12$, and $m = 6$ for Ag, and $\epsilon = 0.012793$ eV, $a = 4.08$ Å, $c = 34.408$, $n = 10$, and $m = 8$ for Au. For given values of n and m the value of c is constant and corresponding results for other metals may be obtained by simply rescaling the units of energy and length.¹ Hence the present calculations for Ag and Au also provide results for SC Rh (12-6) and SC Pt (10-8).

For C₆₀ molecules the intermolecular potential employed is that of Girifalco.² Each molecule is treated as a pseudoatom without orientational coordinates, making the present calculations tractable at the expense of introducing orientational isotropy. The total energy is

$$V_G = -\alpha \sum_{i < j} \left[\frac{1}{s_{ij}(s_{ij}-1)^3} + \frac{1}{s_{ij}(s_{ij}+1)^3} - \frac{2}{s_{ij}^4} \right] + \beta \sum_{i < j} \left[\frac{1}{s_{ij}(s_{ij}-1)^9} + \frac{1}{s_{ij}(s_{ij}+1)^9} - \frac{2}{s_{ij}^{10}} \right], \quad (2)$$

where $s_{ij} = r_{ij}/2a$, r_{ij} being the separation between the centers of mass of molecules i and j , radius a , $\alpha = 3600A/768a^6$, and $\beta = 3600B/368640a^{12}$. A and B are the coefficients of the attractive and repulsive terms in the carbon-carbon Lennard-Jones potential, and were determined² by fitting to the sublimation energy and the lattice constant of bulk C₆₀. The pair well depth and equilibrium separation are then 3218.43 K (0.2773 eV) and 10.0558 Å. The pair well depth is a convenient unit of energy, and most of the results will be presented in this reduced form.

The effective range of the C₆₀ potential is very short compared to the equilibrium pair separation.²⁰ Previous calculations using the same potential predict that the liquid phase of C₆₀ will have either a very limited range of stability or none at all.²⁰⁻²² A study of clusters bound by the Morse potential has revealed how the topology of the potential-energy surface of a finite system changes with the range of the pairwise interaction.²³ Shorter range results in a more complicated surface with more minima and more transition states because distant atoms are insensitive to one another's precise locations. Hence the potential-energy surface becomes glassy or amorphous, as confirmed by other studies.²⁴ Such behavior has also been found in comparisons of C₆₀ and Lennard-Jones clusters.²⁵ Similar considerations can be used to explain the differences observed between C₆₀ and the Sutton-Chen systems found in the following sections.

To simulate a regular fcc lattice a cubic cell of 256 atoms or molecules was used together with the minimum-image convention²⁶ where a given particle interacts with the closest periodic images of the other $N-1$ particles associated with the basic repeated cell. The interaction must be cut off at not more than half the box length for consistency. The Sutton-Chen potential proved more time consuming to evaluate than the C₆₀ and most results are for a cutoff of around 2.5 times the equilibrium bulk nearest-neighbor distance. Calculations were performed to gauge the effects of the cutoff, as described below and in Sec. IX, which were generally inconsequential. Hence, unless stated otherwise, results are for box lengths L and cutoffs C in units of the bulk nearest-neighbor distance given by

SC Ag:	$L = 5.6648$,	$C = 2.5035$,
SC Au:	$L = 5.6569$,	$C = 2.500$,
C ₆₀ :	$L = 5.6568$,	$C = 2.8284$.

For Ag the values were arrived at starting from the ex-

perimental value for L with $C=2.5$ and then relaxing the lattice for the close-packed structure, changing C in proportion to L . For Au the experimental value for L was unchanged by further relaxation, correct to $10^{-2}\%$. For C_{60} L was optimized for the fcc lattice keeping $C=L/2$.

The cutoff and the minimum-image convention introduce a further complication because of discontinuities when a particle passes through the cutoff distance or when the closest periodic image of one particle experienced by another changes. Energy discontinuities could be avoided by employing a fixed neighbor list²⁷ but this was not deemed to be appropriate in the present context of reaction pathway calculations. In fact, discontinuities were not found to pose any serious problems and were only manifested as very small energy jumps in some of the reaction pathways, where the energy should strictly decrease continuously. Such problems were only noticeable for a few of the Sutton-Chen pathways which were checked by steepest descent.

IV. EIGENVECTOR FOLLOWING

Finding transition states on a potential-energy surface is generally a much harder problem than finding minima. Here we define a true transition state²⁸ as a stationary point of Hessian index 1, i.e., with precisely one negative eigenvalue. All the geometry optimizations and reaction path calculations in the present work were performed by eigenvector following.^{29–31} This approach has sufficient flexibility to systematically increase the energy for one degree of freedom, whilst minimizing the energy in all the conjugate directions—the prerequisite for a successful transition-state search. Minima can be found within the same framework by minimizing in all directions.

In fact, some transition states and higher-order saddle points can be located by simple energy minimization. This is possible where the geometry in question is a local minimum within a restricted configuration space defined by the presence of particular symmetry elements. For example, in the nearest-neighbor and second-nearest-neighbor vacancy migrations the transition state has an additional mirror plane passing through the migrating atom that is not present in either of the corresponding minima. Hence the forces which would lead to energy lowering of the transition state through collapse into a minimum vanish by symmetry. Even so, some previous studies of such mechanisms and their analogues in other regular lattices do not appear to perform energy minimization for the transition state,^{10,32} though others do.^{27,5,33–37} In fact, relaxation has often been neglected even for local minima corresponding to vacancies or interstitials,^{38,39} again with some exceptions.^{35,36,40–42} Calculation of lattice defect energies in ionic solids following Mott and Littleton^{43–45} and of energy barriers has employed similar techniques.^{46–49}

However, methods such as damped molecular dynamics^{5,27,50} do not provide a satisfactory general approach to the calculation of transition states. In their study of the generalized saddle surface De Lorenzi, Flynn, and Jacucci refined the transition state using a procedure that employs second derivatives³⁷ and is probably equivalent to

taking Newton-Raphson steps. However, the Newton-Raphson approach is also unsatisfactory because it can converge to a stationary point of any order.²⁹ The saddle surface, which is the hyperplane in which all degrees of freedom except that corresponding to the reaction coordinate defined at the transition state are allowed to vary,^{27,51} is needed when calculating rates by computer simulation at finite temperature. Studies of such surfaces have shown that anharmonic effects make a contribution of less than 2% to the isotope effect factor³⁷ and that corrections due to multiple barrier crossings are negligible at low temperature and reduce the rate by only around 10% at the melting point.⁵⁰ Conjugate-gradient techniques were employed by De Vita and Gillan³⁵ to calculate the vacancy and nearest-neighbor migration energies in Al, but such optimizations can also converge to saddle points rather than minima.⁵² Perkins and DePristo⁵³ have used the Ulitsky-Elber algorithm⁵⁴ in recent surface calculations which include rearrangement pathways for hundreds of active atoms. It would be interesting to compare the performance of the above method, which does not require second derivatives, with eigenvector following in future work.

We now consider the eigenvector-following approach in more detail. Refinements of this method have improved the convergence properties and made possible calculations for systems with hundreds of degrees of freedom.^{55–57} In fact, the present approach is especially simple for a bulk system, and to appreciate this some understanding of the method is needed. The standard Newton-Raphson step is given by

$$\mathbf{h}_{\text{NR}} = -\mathbf{H}^{-1}\mathbf{g} \quad (3)$$

However, the inverse Hessian does not exist, because \mathbf{H} will usually have zero eigenvalues corresponding to bulk translations and rotations. For isolated molecules there are six zero eigenvalues at a stationary point,⁵⁸ while for an extended system there are only three corresponding to the bulk translations.

It is helpful to consider the consequences of the Newton-Raphson step in the basis of Hessian eigenvectors \mathbf{V}_i where the corresponding eigenvalues are b_i . The step and energy change are then²⁵

$$\mathbf{h}_{\text{NR}} = -\sum_i \frac{F_i \mathbf{V}_i}{b_i} \quad \text{and} \quad \Delta E_{\text{NR}} = -\sum_i \frac{F_i^2}{2b_i} \quad (4)$$

where F_i is the component of the gradient along \mathbf{V}_i . If the number of zero eigenvalues were constant we could employ the Newton-Raphson step using (4), taking only contributions from degrees of freedom with $b_i \neq 0$. However, at a general, nonstationary point the rotations are coupled to vibrations by terms linear in the gradient.⁵⁸ Hence, for a free molecule there are always three zero eigenvalues corresponding to the translational normal modes, but there are generally a number of other modes with small but nonzero eigenvalues. For a bulk system, however, there are always three, and only three, zero eigenvalues at an arbitrary point,⁵⁹ and so we can perform geometry optimizations in Cartesian coordinates without further complications.

Although the above arguments relate to the Newton-Raphson step they carry over to the present eigenvector-following calculations, which employed steps of the form

$$h_i = \frac{\pm 2F_i}{|b_i|(1 + \sqrt{1 + 4F_i^2/b_i^2})}, \quad (5)$$

where the plus is for maximization, and the minus for minimization. In most transition-state searches the eigenvector corresponding to the smallest Hessian eigenvector was followed uphill. Analytic first and second derivatives of the energy were employed at every step, and the resulting stationary-point energies and geometries are essentially exact for the model potentials in question. Calculations were considered converged when the root-mean-square force was less than 10^{-5} and the maximum step size less than 10^{-4} for two successive steps, where the units of energy and distance are eV and the nearest-neighbor distance for the Sutton-Chen potentials, and the pair well depth and 3.469 Å for C_{60} , the latter being the value of the Lennard-Jones σ parameter for carbon-carbon interactions.² All stationary points were characterized by their normal-mode frequencies.

Some of the stationary points calculated in the present work are neither minima nor true transition states but higher-index saddle points with more than one negative Hessian eigenvalue. These were found using a pseudo-Newton-Raphson step employing h_i defined in (5) but always taking the minus sign and the actual value of b_i , rather than the modulus, in the denominator.

To visualize the mechanisms and reaction pathways, the transition-state geometries were perturbed by adding (and subtracting) a small fraction of order 0.01 of the normalized eigenvector corresponding to the unique negative Hessian eigenvalue, and initiating eigenvector-following searches for minima from the resulting geometries. Smaller displacements were needed for some of the highly localized mechanisms. The pathways calculated in this way do not follow true steepest-descent lines because the eigenvector-following step is not strictly parallel to the gradient vector. However, they should be quite adequate for the present purposes.^{25(c)}

V. CHARACTERIZING REARRANGEMENT PATHWAYS

Various properties of the reaction paths were calculated to provide comparisons between the different systems and to give quantitative measures of path length and cooperativity. The integrated path length S is the arc length in $3N$ -dimensional configuration space, where N is the number of atoms or molecules in the periodically repeated cell. S was approximated as a sum over eigenvector-following steps:

$$S = \sum_{\text{steps}} \left[\sum_i \Delta Q_i^2 \right]^{1/2}, \quad (6)$$

where ΔQ_i is the step along Hessian eigenvector i . Clearly the distance between minima s and t in nuclear configuration space⁶⁰ D must be less than S , where

$$D = \left[\sum_i [Q_i(s) - Q_i(t)]^2 \right]^{1/2}, \quad (7)$$

and $Q_i(s)$ is the value of the nuclear Cartesian coordinate Q_i for minimum s , etc.

The moment ratio of displacement γ provides a measure of how cooperative a rearrangement is:⁶¹

$$\gamma = \frac{N \sum_i [Q_i(s) - Q_i(t)]^4}{\left[\sum_i [Q_i(s) - Q_i(t)]^2 \right]^2}. \quad (8)$$

If only a single atom moves then $\gamma = N$ and the rearrangement is entirely localized, whereas if all atoms move through the same distance then $\gamma = 1$ and the process is completely cooperative. Some previous comparisons of these quantities for clusters bound by the Lennard-Jones and Girifalco C_{60} potentials are provided elsewhere.^{25(c)} For the present calculations the nearest periodic image was always used in calculating distances.

Defect formation energies were all calculated by comparison with the regular fcc lattice of 256 particles by rescaling the energy. Hence, if the defect structure has N' particles, where $|N' - 256| \leq 3$ in this study, and energy $E_{N'}$, then the formation energy E^F was estimated as

$$E^F \approx \frac{256}{N'} E_{N'} - E_{256} \quad (9)$$

(which gives essentially the same result as $E_{N'} - N'E_{256}/256$). Comparison is therefore made with a reference state consisting of the regular lattice with the same number of particles, rather than with a surface state. For the SC potentials the results of this approach are practically the same as those of Uppenbrink, Johnston, and Murrell,¹⁵ who used a different definition. Expression (9) was employed by Denteneer and Soler³⁶ and is slightly different from that used by De Vita and Gillan,³⁵ where the volume is adjusted too.

For C_{60} Girifalco has previously estimated the vacancy formation energy as half the sublimation energy, arguing that half the contacts lost when a bulk molecule is removed are recovered when it is placed on the surface. However, the latter process involves six nearest-neighbor contacts, as does the sublimation energy within the same approximation. Professor Girifalco has confirmed to the authors that the previous factor of one-half was incorrect.² The approach used in the present work gives a value that is practically the same as taking the full sublimation energy.

VI. VACANCIES AND VACANCY MIGRATION MECHANISMS

A. Minima

Tables I and II collect the energies of the regular fcc lattice, the unique single-vacancy minimum, and various two- and three-vacancy minima. The nomenclature for the divacancy structures, which have 254 atoms or molecules in the cubic cell, is illustrated in Fig. 1: for the structures referred to as 254A-F the vacancies, in units of the nearest-neighbor distance, lie in the following representative positions.

TABLE I. Minima found for the fcc lattice and structures with vacancies for the Sutton-Chen potentials. Energies are in eV. ΔE is the energy relative to the 256-atom fcc structure in units of the cohesive energy and E^F is the formation energy in eV calculated by rescaling the number of atoms and comparing with the perfect lattice as described in the text. For the fcc lattice E^F is the cohesive energy per atom.

Structure	Energy	ΔE	E^F	Energy	ΔE	E^F
			SC Ag			
256 fcc	-743.768 568		2.905	-965.417 381		3.771
255 vacancy	-739.879 751	1.339	0.987	-960.983 336	1.176	0.665
254 A	-736.001 993	2.673	1.971	-956.538 718	2.354	1.347
254 B	-735.987 304	2.678	1.986	-956.541 315	2.354	1.344
254 C	-735.989 724	2.677	1.984	-956.545 269	2.353	1.340
254 D	-736.088 791	2.643	1.884	-956.602 413	2.337	1.283
254 E	-735.987 661	2.678	1.986	-956.537 369	2.355	1.348
254 F	-735.991 609	2.677	1.982	-956.548 365	2.352	1.337
253 A A 1	-732.123 855	4.008	2.963	-952.093 737	3.533	2.034
253 A A 2	-732.120 520	4.009	2.967	-952.085 714	3.535	2.042
253 B B 1	-732.094 311	4.018	2.993	-952.098 118	3.532	2.030
253 B B 2	-732.092 761	4.019	2.995	-952.093 492	3.533	2.034
253 D D 1	-732.299 798	3.948	2.785	-952.220 099	3.500	1.906
253 D D 2	-732.402 080	3.912	2.682	-952.293 473	3.480	1.832

Label	Vacancy separation	Vacancy coordinates
D	1	(0,0,0), (1/√2, 1/√2, 0)
A	√2	(0,0,0), (√2, 0, 0)
E	√3	(0,0,0), (√2, 1/√2, 1/√2)
B	2	(0,0,0), (√2, 0, √2)
F	√5	(0,0,0), (0, 3/√2, 1/√2)
C	√6	(0,0,0), (√2, √2, √2)

For trivacancy structures six arrangements were considered initially; the positions of the empty sites, in units of the nearest-neighbor distance, are

TABLE II. Minima found for the fcc lattice and structures with vacancies for C_{60} . The unit of energy is the pair well depth. ΔE is the energy relative to the 256-atom fcc structure in units of the cohesive energy and E^F is the formation energy in units of the pair well depth calculated by rescaling the number of atoms and comparing with the perfect lattice as described in the text. For the fcc lattice E^F is the cohesive energy per molecule.

Structure	Energy	ΔE	E^F
256 fcc	-1655.842 670		6.468
255 vacancy	-1642.908 056	2.000	6.492
254 A	-1630.039 392	3.989	12.968
254 B	-1629.978 769	3.999	13.029
254 C	-1629.974 889	3.999	13.033
254 D	-1630.973 382	3.845	12.027
254 E	-1629.988 104	3.997	13.020
254 F	-1629.976 278	3.999	13.032
253 A A 1	-1617.171 250	5.979	19.495
253 A A 2	-1617.159 243	5.978	19.491
253 B B 1	-1617.049 914	5.998	19.618
253 B B 2	-1617.049 402	5.998	19.619
253 D D 1	-1619.044 285	5.689	17.600
253 D D 2	-1620.037 947	5.536	16.595

A A 1	(0,0,0), (√2, 0, 0), (-√2, 0, 0)
A A 2	(0,0,0), (√2, 0, 0), (0, 0, √2)
B B 1	(0,0,0), (√2, 0, √2), (-√2, 0, √2)
B B 2	(0,0,0), (√2, 0, √2), (-√2, 0, -√2)
D D 1	(0,0,0), (1/√2, 1/√2, 0), (-1/√2, -1/√2, 0)
D D 2	(0,0,0), (1/√2, 1/√2, 0), (0, 1/√2, 1/√2)

There are some interesting patterns discernible in Tables I and II. First we note that the cohesive energies per atom or molecule should all be in good agreement

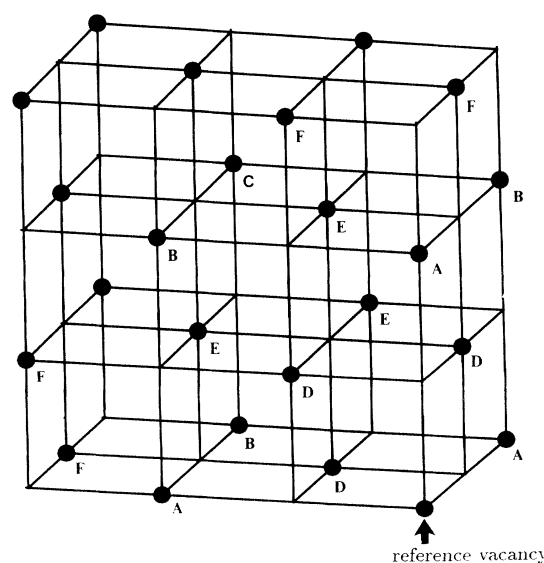


FIG. 1. Labeling scheme for divacancy structures. The first vacancy is at the bottom right-hand corner site and the labels A-F then refer to the position of the second vacancy with respect to this site.

TABLE III. Rearrangement pathways for SC Ag involving vacancy migration. Energies are all in eV. MIN1 and MIN2 are the two minima, Δ_1 and Δ_2 are the two barriers. S , D , and γ are defined in Sec. V and ω is the magnitude of the unique imaginary normal-mode frequency of the transition state in cm^{-1} .

MIN1	Δ_1	TS	Δ_2	MIN2	S (Å)	D (Å)	γ	ω	
255 vacancy	0.7334	$\langle 110 \rangle$	−739.146 307	0.7334	255 vacancy	3.40	2.85	252.4	58.1
255 vacancy	3.1721	$\langle 100 \rangle$	−736.707 674	3.1721	255 vacancy	5.67	4.09	252.6	86.8
254D	0.4039		−735.684 898	0.4039	254D	3.57	2.85	251.0	14.7
254B	0.6572		−735.330 140	0.7587	254D	3.40	2.87	251.3	57.7
254D	0.7591		−735.329 644	0.6580	254E	3.35	2.86	251.2	56.7
254F	0.7292		−735.262 376	0.7396	254A	3.41	2.84	251.4	58.2
254F	0.7319		−735.259 691	0.7319	254F	3.43	2.85	251.4	57.9
254C	0.7324		−735.257 362	0.7303	254E	3.41	2.85	251.4	57.8
253DD2	0.2146		−732.187 518	0.2146	253DD2	3.44	2.71	250.3	33.8
253DD1	0.4203		−731.879 457	0.3127	253BE1 ^a	3.75	2.80	249.9	21.6
253DD1	0.7208		−731.491 051	0.8087	253AD1 ^b	3.48	2.86	250.3	59.1
253AA1	0.7031		−731.420 758	0.6889	253AE1 ^c	3.43	2.83	250.4	56.4
253AA2	0.7075		−731.413 052	0.8867	253DD1	3.53	2.87	250.1	60.6
253BG1 ^d	0.7334		−731.362 958	0.7314	253BB1	3.43	2.85	250.4	57.9
253BB2	4.7635		−727.331 114	4.7616	253BG2 ^e	9.97	6.44	70.0	34.3

^a $E = -732.211\,891$.

^bVacancy moves from $(-1/\sqrt{2}, -1/\sqrt{2}, 0)$ to $(0, -\sqrt{2}, 0)$, $E = -731.192\,196$.

^cVacancy moves from $(-\sqrt{2}, 0, 0)$ to $(-\sqrt{2}, 1/\sqrt{2}, -1/\sqrt{2})$, $E = -732.109\,667$.

^dVacancy moves from $(-\sqrt{2}, 1/\sqrt{2}, 3/\sqrt{2})$, $E = -732.094\,311$, to $(-\sqrt{2}, 0, \sqrt{2})$.

^eVacancy moves from $(-\sqrt{2}, 0, -\sqrt{2})$ to $(-3/\sqrt{2}, 1/\sqrt{2}, -\sqrt{2})$, $E = -732.092\,761$.

with experiment because this property was fitted in each case. The energy difference between a defect structure and the ideal lattice is about 1.3 and 1.2 times the cohesive energy per atom for each vacancy in Ag and Au, respectively. For C_{60} , however, the energy increase for each vacancy is close to twice the ideal cohesive energy.

If we neglect the effects of relaxation of the surrounding atoms upon vacancy formation and count only nearest-neighbor interactions, which each contribute E_{NN} , then the increase in energy for each vacancy created would be roughly $12E_{\text{NN}}$. However, in the same approximation the cohesive energy per atom is $6E_{\text{NN}}$, and

TABLE IV. Rearrangement pathways for SC Au involving vacancy migration. Energies are all in eV. MIN1 and MIN2 are the two minima, Δ_1 and Δ_2 are the two barriers. S , D , and γ are defined in Sec. V and ω is the magnitude of the unique imaginary normal-mode frequency of the transition state in cm^{-1} .

MIN1	Δ_1	TS	Δ_2	MIN2	S (Å)	D (Å)	γ	ω	
255 vacancy	0.5658	$\langle 110 \rangle$	−960.417 149	0.5658	255 vacancy	3.36	2.83	252.1	38.4
255 vacancy	2.4393	$\langle 100 \rangle$	−958.544 042	2.4393	255 vacancy	5.64	4.06	252.3	58.6
254D	0.3784		−956.223 997	0.3784	254D	3.44	2.81	251.3	18.6
254B	0.5188		−956.022 495	0.5799	254D	3.38	2.85	251.2	38.0
254D	0.5757		−956.026 790	0.5106	254E	3.40	2.83	251.2	37.5
254F	0.5811		−955.967 247	0.5715	254A	3.39	2.83	251.0	38.7
254F	0.5613		−955.989 023	0.5613	254F	3.38	2.82	251.1	38.1
254C	0.5701		−955.975 145	0.5622	254E	3.39	2.83	251.0	38.2
253DD2	0.3784		−956.223 997	0.3784	253DD2	3.44	2.81	251.3	18.6
253DD1	0.3954		−951.824 690	0.3230	253BE1 ^a	3.67	2.82	250.4	18.4
253DD1	0.5537		−951.602 818	0.6173	253AD1 ^b	3.40	2.82	250.2	39.1
253A A1	0.5321		−951.561 613	0.5291	253AE1 ^c	3.36	2.80	250.0	37.1
253A A2	0.5451		−951.540 587	0.6795	253DD1	3.44	2.82	250.1	40.3
253BG1 ^d	0.5612		−951.536 952	0.5635	253BB1	3.39	2.83	250.1	38.1
253BB2	3.6183		−948.475 161	3.6221	253BG2 ^e	10.75	6.40	69.9	24.6

^a $E = -952.156\,537$.

^bVacancy moves from $(-1/\sqrt{2}, -1/\sqrt{2}, 0)$ to $(0, -\sqrt{2}, 0)$, $E = -952.156\,537$.

^cVacancy moves from $(-\sqrt{2}, 0, 0)$ to $(-\sqrt{2}, 1/\sqrt{2}, -1/\sqrt{2})$, $E = -952.090\,692$.

^dVacancy moves from $(-\sqrt{2}, 1/\sqrt{2}, 3/\sqrt{2})$, $E = -952.100\,480$, to $(-\sqrt{2}, 0, \sqrt{2})$.

^eVacancy moves from $(-\sqrt{2}, 0, -\sqrt{2})$ to $(-3/\sqrt{2}, 1/\sqrt{2}, -\sqrt{2})$, $E = -952.097\,256$.

TABLE V. Rearrangement pathways for C_{60} involving vacancy migration. Energies are all in units of the pair well depth. MIN1 and MIN2 are the two minima, Δ_1 and Δ_2 are the two barriers. S , D , and γ are defined in Sec. V and ω is the magnitude of the unique imaginary normal-mode frequency of the transition state in cm^{-1} .

MIN1	Δ_1	TS	Δ_2	MIN2	S (Å)	D (Å)	γ	ω
255 vacancy	22.6488	$\langle 110 \rangle$ -1620.259 280	22.6488	255 vacancy	12.46	10.01	253.0	20.3
255 vacancy	115.9795	$\langle 110 \rangle$ -1526.928 518	115.9795	255 vacancy	22.41	14.18	253.0	32.3
254D	9.6068	-1621.367 303	0.5203	254 off-center ^a	6.90	5.94	251.6	12.5
254B	21.6631	-1608.315 269	22.6577	254D	12.30	10.02	252.0	20.2
254D	22.6589	-1608.314 505	21.6736	254E	12.42	10.01	252.0	20.2
254F	22.5739	-1607.402 391	22.6370	254A	12.50	10.01	252.0	20.3
254F	22.5745	-1607.401 751	22.5745	254F	12.50	10.01	252.0	20.2
254C	21.6592	-1607.374 904	22.6132	254E	12.41	10.01	252.0	20.3
253DD2	4.4092	-1615.628 759	4.4092	253DD2	11.89	9.98	251.0	7.0
253BE1 ^b	8.6577	-1609.401 040	0.5515	253 off-center ^c	6.61	5.95	230.4	12.6
253DD1	22.6628	-1596.381 509	21.7259	253AD1 ^d	12.35	10.02	251.0	20.0
253AA2	20.8007	-1596.358 517	22.6858	253DD1	12.21	10.02	251.0	19.6
253AA1	21.9644	-1595.079 849	22.0397	253AE1 ^e	12.39	10.01	251.0	19.9
253BG1 ^f	22.5052	-1594.539 873	22.5100	253BB1	12.45	10.01	251.0	20.2
253BH1 ^g	128.5483	-1488.496 687	128.5474	253BI1 ^h	26.85	17.33	138.9	25.3

^a $E = -1629.978\,769$.

^b $E = -1618.058\,710$.

^c $E = -1609.952\,493$.

^dVacancy moves from $(-1/\sqrt{2}, -1/\sqrt{2}, 0)$ to $(0, -\sqrt{2}, 0)$, $E = -1618.107\,455$.

^eVacancy moves from $(-\sqrt{2}, 0, 0)$ to $(-\sqrt{2}, 1/\sqrt{2}, -1/\sqrt{2})$, $E = -1617.119\,507$.

^fVacancy moves from $(-\sqrt{2}, 1/\sqrt{2}, 3/\sqrt{2})$, $E = -1617.045\,118$, to $(-\sqrt{2}, 0, \sqrt{2})$.

^gVacancy moves from $(2/\sqrt{2}, 3/\sqrt{2}, -3/\sqrt{2})$, $E = -1617.045\,031$, to $(2\sqrt{2}, \sqrt{2}, -\sqrt{2})$, $E = -1617.044\,128$, with two common vacancies at $(0, 0, 0)$ and $(\sqrt{2}, 0, \sqrt{2})$.

so the energy increase for each vacancy is twice the cohesive energy. C_{60} actually follows this scheme quite accurately, indicating that there is little relaxation around vacancies for this short-range potential. For Ag and Au, however, relaxation lowers the energy difference significantly. It is important to notice that formation of multiple vacancies is most favorable when they occupy adjacent lattice sites because fewer nearest-neighbor interactions are lost. Hence, for all three systems minimum 254D is the lowest-energy divacancy structure, and minima 253DD2 and 253DD1 are the lowest-energy trivacancies.

For the largest vacancy separation, in structure 254C, the energy difference is very close to that expected for two single defects. This observation provides evidence that the number of particles in the basic unit is sufficiently large for at least some of the results to be independent of the periodic boundary conditions.

Details of the pathways found involving vacancy migrations are collected in Tables III–V. The results for SC Ag and Au are generally analogous; transition-state searches were first performed for Au and then optimizations for Ag were started from the converged Au geometries. All the transition states reported in Table II converged within a few steps from the appropriately scaled Au geometries. The energetic ordering of the transition states is the same for the trivacancy structures, but a little different for the divacancies; the magnitude of the unique imaginary frequency is usually 1.5 times larger for Ag.

B. Rearrangement mechanisms

Most of the rearrangements can be described as nearest-neighbor single-vacancy migrations. For all but the last process in Tables III–V the mechanism is essentially localized on one particle ($\gamma \approx N$) and in most cases D is practically equal to the nearest-neighbor distance (2.89 Å for Ag, 2.88 Å for Au, and 10.04 Å for C_{60}). The barriers are generally quite similar too, i.e., around 0.7 eV, 0.55 eV, and 22 times the pair well depth for Ag, Au, and C_{60} , respectively. The basic $\langle 110 \rangle$ nearest-neighbor migration for SC Ag is illustrated in Fig. 2.

For each potential there are one divacancy and two trivacancy processes with particularly low barriers, and these are analyzed in detail below. In each case the transition state has several vacant lattice sites adjacent to the migrating atom, which does not follow an approximately straight-line path. Instead it is deflected towards an adjacent “spectator” vacancy, lowering the energy of the transition state by increasing the number of interactions with nearest neighbors of the empty sites.

All the illustrations of rearrangement pathways were prepared using Ref. 62. In each case the two minima appear at the extreme left and right, with the transition state in the middle and two intermediate structures from the reaction pathway on either side. The transition vector, i.e., the Hessian eigenvector corresponding to the unique negative Hessian eigenvalue, is superimposed upon the transition state in the appropriate sense for the rearrangement from left to right. The relative heights of

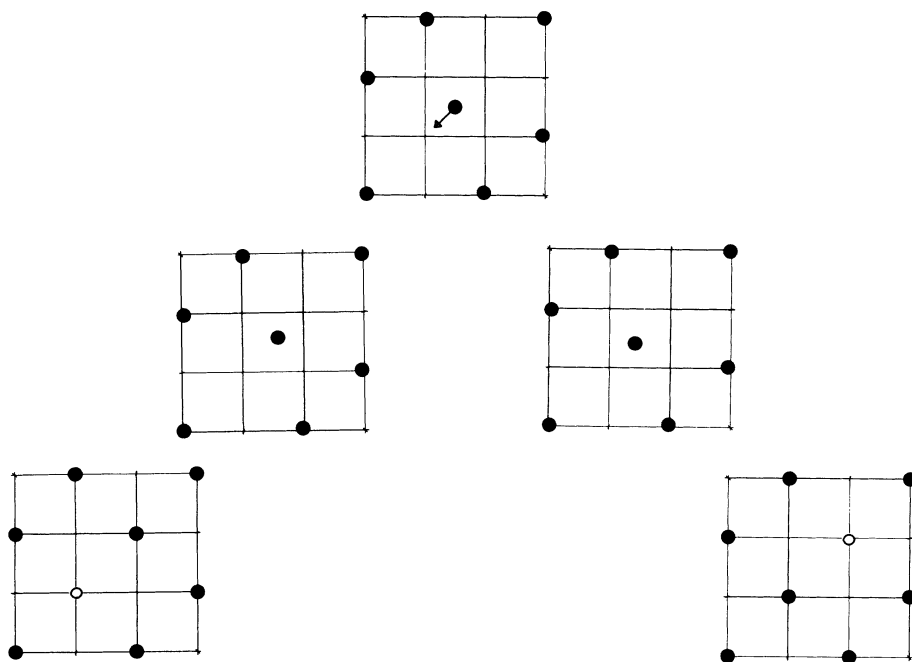


FIG. 2. Nearest-neighbor vacancy migration for SC Ag viewed in a section of the (001) plane; the vacancy positions in the two minima are marked by open circles.

the five frames are chosen to reflect the energies of the configurations in a schematic fashion. In each case a section is taken through either the (001) or (111) plane, as appropriate. For (001) projections a simple cubic grid is added to guide the eye and vacancies are explicitly marked by open circles.

The mechanism for second-nearest-neighbor vacancy migration is illustrated in Fig. 3. Here migration occurs in a $\langle 100 \rangle$ rather than a $\langle 110 \rangle$ direction, and at constant volume the barrier is about 4.3 times higher for Ag and Au, and five times higher for C_{60} , because the particle must squeeze through a smaller gap, causing more disruption. Both the first- and second-nearest-neighbor vacancy migrations are symmetrical in that the two sides of the pathway leading away from the transition state are equivalent.

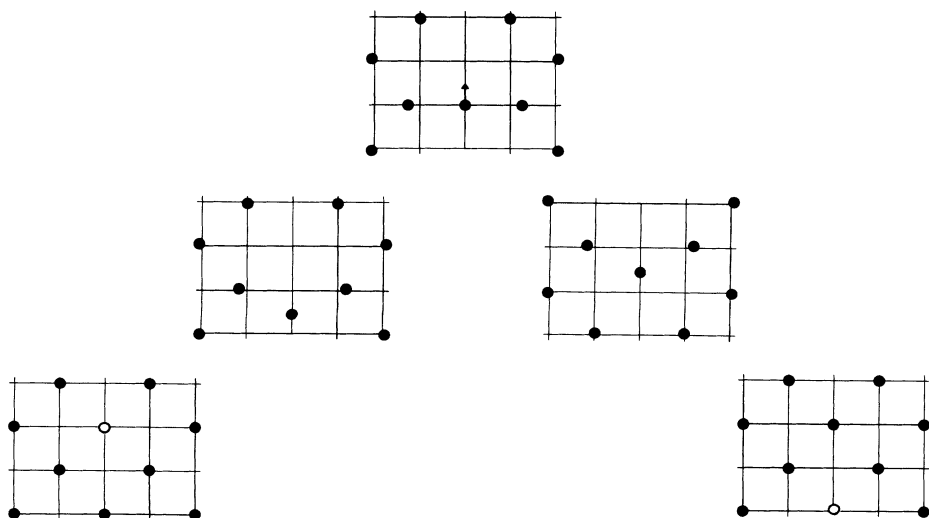


FIG. 3. Second-nearest-neighbor vacancy migration for SC Ag viewed in a section of the (001) plane; the vacancy positions in the two minima are marked by open circles.

For the divacancies the rearrangement of the 254D nearest-neighbor vacancy pair which leads to a different 254D-type structure has lower barriers than any of the other mechanisms. For Ag and Au the barrier is some 0.3 and 0.2 eV lower than the usual value, while for C_{60} the corresponding process involves a new, relatively high-energy minimum and is asymmetrical. The mechanism for Ag and Au is illustrated in Fig. 4. Note from Tables III and IV that the integrated path length S is slightly larger than expected for a direct motion, and Fig. 4 confirms that in the transition state the migrating atom moves away from the straight-line path in the direction of the neighboring vacancy. Although the transition state appears to have a threefold rotation axis, inspection of the distances reveals that there is actually only a plane of symmetry perpendicular to the transition vector. In fact,

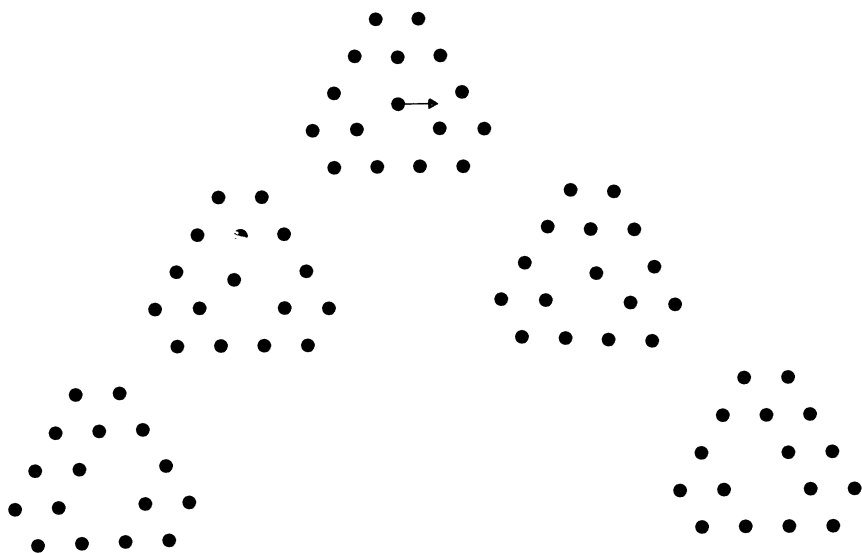


FIG. 4. Rearrangement of the 254D divacancy structure for Ag to give an equivalent minimum viewed in a section of the (111) plane.

there cannot be a threefold axis because of the McIver-Stanton geometric selection rules⁶³ which state that the transition vector must transform into plus or minus itself under any symmetry operation of the system. This would not be possible if there were a true threefold axis. For C_{60} the transition-state geometry in Ag and Au roughly corresponds to a high-energy minimum (Fig. 5). The McIver-Stanton rules do not prevent the minimum from having higher symmetry, and indeed the off-site molecule lies on a $\langle 111 \rangle$ -type axis, equidistant from the three unoccupied sites.

There are two trivacancy rearrangements with particularly low barriers and one with particularly high barriers for each system, the latter corresponding to significant motion of more than one particle. The rearrangement of

minimum 253DD2 to give an equivalent structure, which contains three vacancies in a triangle, is common to all three systems and is illustrated in Fig. 6. In the transition state the migrating particle is not equidistant from the tetrahedron of nearest-neighbor vacant sites but is attracted away from the straight-line path between sites towards the spectator vacancies, as for the rearrangement of the 254D structure.

The trivacancy structure with a particle in the center of a tetrahedron of empty lattice sites was also investigated for comparison with previous work.⁴² For all three systems this structure corresponds to a stationary point of Hessian index 3; the energies are given in Table VI. The previous calculations considered the Lennard-Jones potential and a Morse potential parametrized for Cu, and

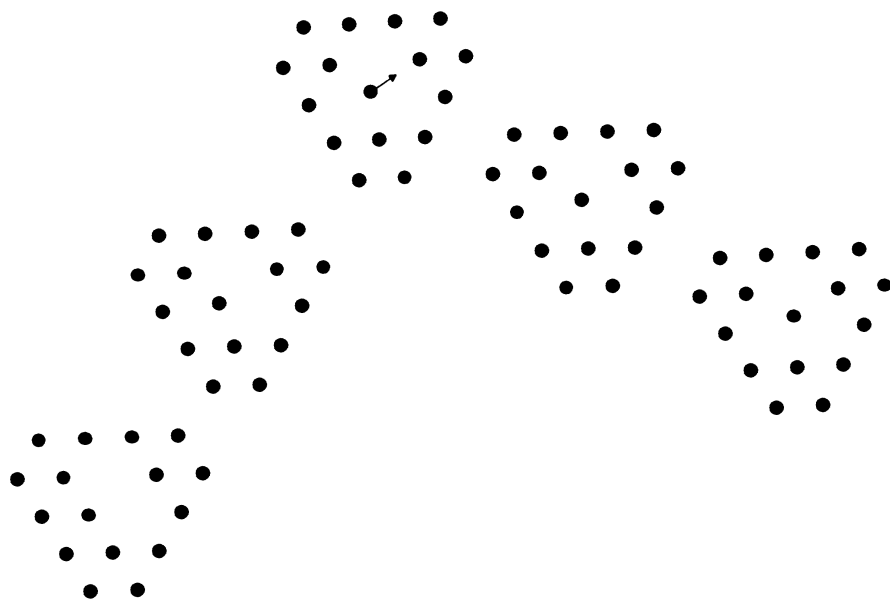


FIG. 5. Rearrangement between the 254D structure for C_{60} and a high-energy divacancy minimum with an off-site molecule viewed in a section of the (111) plane.

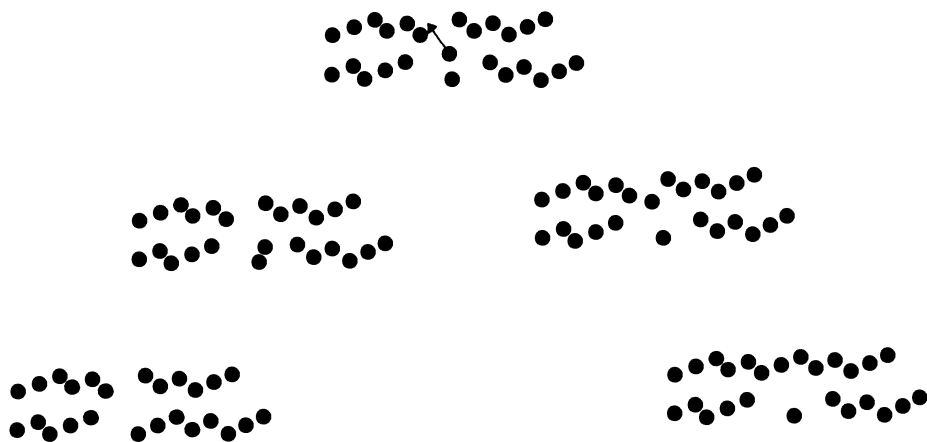


FIG. 6. Rearrangement of the 253DD2 trivacancy minimum for C_{60} to give an equivalent structure. An atom migrates between two (111)-type planes so that the lower plane contains all three vacancies in the final minimum.

found that the symmetrical structure was stable for the latter but not for the former.⁴² A calculation for the Lennard-Jones potential was performed for comparison using box length 5.6569 and cutoff 2.5 in units of the nearest-neighbor distance. Again the symmetrical structure had Hessian index 3.

The stability found for the Morse potential in the previous study is more puzzling.⁴² This potential has only one adjustable parameter, ρ_0 , corresponding to the range of the interaction.²³ Values of $\rho_0 = 6$ and 13.6160... are obtained by fitting the Morse potential to the Lennard-Jones and Girifalco forms, the larger ρ_0 corresponding to short range, and both of these potentials give saddle points for the symmetrical vacancy cluster. Unfortunately, the parameters used in the previous study were not reported.⁴² To check that relaxation does not change the number of negative eigenvalues in the present work the geometries were reoptimized for all four potentials, maintaining the same ratio of the box length to the cutoff. In each case the Hessian index 3 was retained after relaxation.

The other trivacancy pathway with small barriers involves the 253DD1 minimum for Ag and Au, with three nearest-neighbor vacancies in a line. The second minimum has *B*- and *E*-type vacancies at nearest-neighbor positions, and is common to Ag, Au, and C_{60} . For Ag and Au the mechanism is analogous to that illustrated for the 254D divacancy rearrangement (Fig. 7). Hence, just as for the 254D process, the migrating atom deviates from a straight-line path towards a neighboring vacancy. The analogy carries over to C_{60} , where instead of 253DD1 we find an off-center molecule practically equidistant from three vacant lattice sites in the second minimum (Fig. 8).

The rearrangement of the 254D divacancy is the

lowest-energy divacancy diffusion mechanism, although the corresponding process in C_{60} would proceed via a new high-energy minimum according to the Girifalco potential. Searches were also conducted for a divacancy migration in which two nearest-neighbor atoms move simultaneously into adjacent vacancies. For all three potentials a saddle of Hessian index 2 was found close to the idealized geometry for this process. Following both of the downhill directions in each sense produced three 254D-type structures, with the vacancies in different positions, and one minimum of type 254E. The connectivity is shown in Fig. 9. Lower-energy pathways exist between these four minima via single-vacancy, nearest-neighbor mechanisms, in accordance with the Murrell-Laidler theorem.²⁸

De Lorenzi and Ercolessi³³ report a stationary point of Hessian index 2 corresponding to a double-jump vacancy migration in their calculations for Au.⁶⁴ Using trial and error saddle searches they describe a process in which two nearest neighbors move together in a $\langle 110 \rangle$ direction so that a vacancy effectively moves through two nearest-neighbor distances. If such a saddle point does exist then there must be a lower-energy pathway involving only true transition states connecting the same two minima. In fact, we were unable to find a stationary point of the appropriate geometry for SC Ag and searches were not attempted for the other potentials. Hence, if true transition states exist for concerted multiple-jump processes, then they have yet to be characterized.

From the summary in Table X below we see that after the nearest-neighbor vacancy migration mechanism, the divacancy migration (involving structure 254D) has the lowest combined formation and migration energy. Hence the present calculations suggest that, if a second mecha-

TABLE VI. Energy of the trivacancy stationary point consisting of a tetrahedron of empty sites with a particle in the middle. In each case the structure has Hessian index 3. The units are eV for Ag and Au and the pair well depth for C_{60} and the Lennard-Jones (LJ) potential.

	SC Ag	SC Au	C_{60}	LJ
Unrelaxed	-732.163 428	-951.751 863	-1614.617 178	-1998.276 814
Relaxed	-732.184 261	-951.800 110	-1614.620 324	-2038.008 969

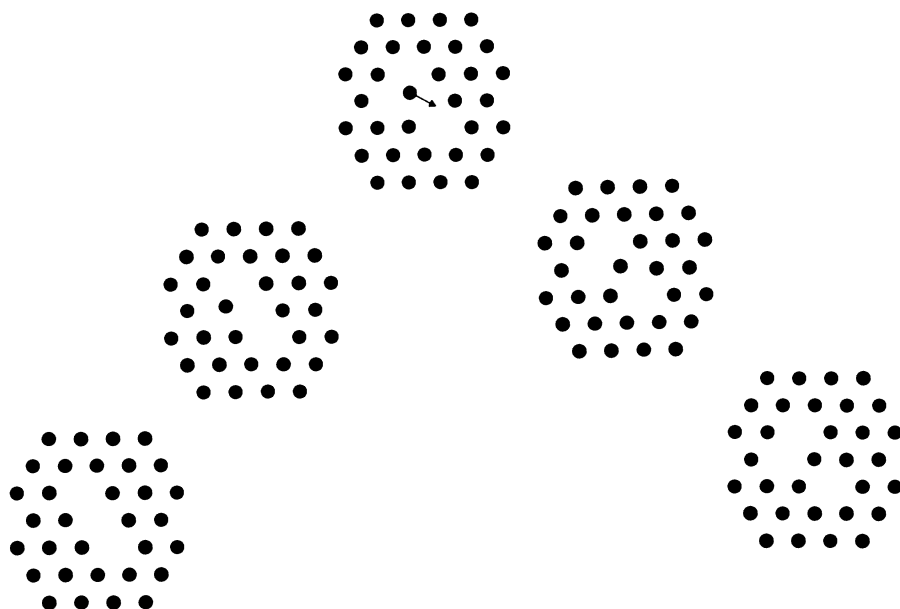


FIG. 7. Rearrangement of 253DD1 for SC Ag to the higher-energy minimum 253EB1 viewed in a section of the (111) plane.

nism is responsible for the upward curvature of Arrhenius plots at high temperature, then it is probably the divacancy process. For C_{60} , the divacancy mechanism actually appears to be more favorable than the single-vacancy process. The relaxation energies for these two rearrangements are both small (Sec. IX).

VII. INTERSTITIAL MIGRATION MECHANISMS

The first mechanism investigated here was the formation of a vacancy-interstitial pair, or Frenkel defect.⁶⁵ For Au we found a rearrangement where three second-nearest-neighbor atoms migrate in a line to give a $\langle 100 \rangle$ split interstitial whose center is separated by $2\sqrt{2}$ times the nearest-neighbor distance from a vacancy (Fig. 10). For Ag the stationary point corresponding to the Au transition state has Hessian index 3 ($E = -738.862\,363$ eV). However, there is a true transition state corresponding to a small perturbation of this structure where the

three atoms move off axis. The higher-energy minimum has a $\langle 100 \rangle$ split interstitial whose center is separated by $\sqrt{5}$ times the nearest-neighbor distance from a vacancy (Fig. 11). The axis of the split interstitial is perpendicular to that found in the Au analogue, providing the first qualitative difference found between the two potentials in this study.

C_{60} is different from both Ag and Au. As for Au there is a rearrangement in which three second nearest neighbors move in a $\langle 100 \rangle$ direction. However, instead of a vacancy-split-interstitial pair we find a vacancy and an interstitial molecule in an octahedral site separated by $3/\sqrt{2}$ nearest-neighbor distances (Fig. 12). The energetics of all these pathways are summarized in Table VII. This result is indicative of the unfavorable nature of split interstitials in C_{60} with the present potential.

The remaining results in this section are all for cubic cells containing 257 particles. The mechanisms found for interstitial migration are different for the three potentials.

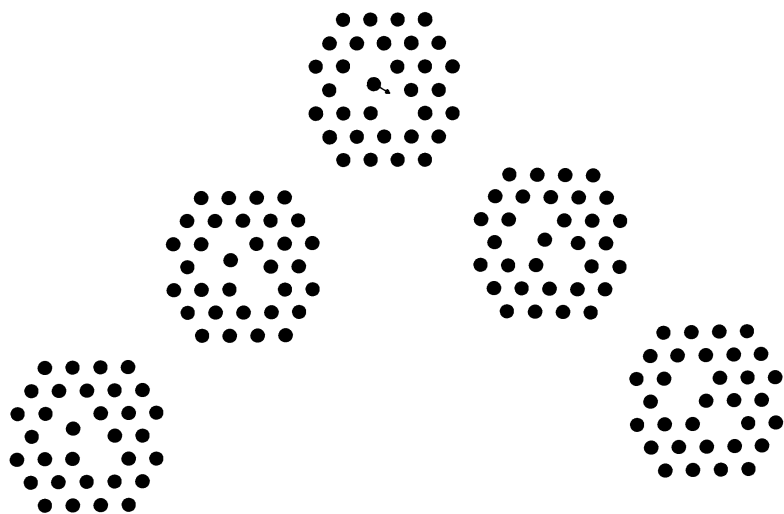


FIG. 8. Rearrangement from a minimum with an off-center molecule to minimum 253EB1 for C_{60} viewed in a section of the (111) plane.

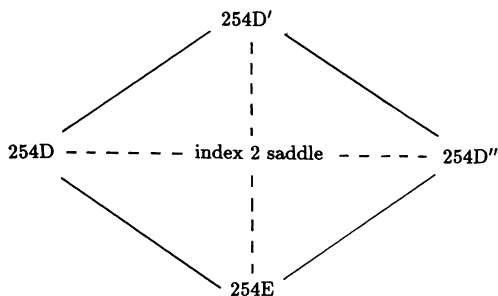


FIG. 9. Schematic connectivity around the index-2 saddle found when searching for a double-jump mechanism. Solid lines indicate connections via a simple transition state and dashed lines represent steepest-descent paths from the index-2 saddle. The lowest-energy path between any two minima circumnavigates the higher-order saddle.

For SC Ag the $\langle 100 \rangle$ split interstitial can move via a relatively cooperative process involving rotation of a pentagon of atoms (Fig. 13). The axis of the interstitial dumbbell rotates through 90° in this mechanism, while the center of the interstitial moves through one nearest-neighbor distance. This resembles the mechanism suggested by Bocquet in the context of Ag-Zn solid solutions.⁶⁶

For Au, however, we found a rearrangement between the $\langle 100 \rangle$ split interstitial and an O_h interstitial which occurs primarily through the motion of three atoms in a line (Fig. 14). For SC Ag the corresponding O_h interstitial is a saddle point of index 3 ($E = -742.783\,605$ eV). Performing a transition-state search from the rescaled Ag geometry with the SC Au potential gives the O_h -to- $\langle 100 \rangle$ rearrangement again. Clearly these mechanisms

are related to those found above for the formation of vacancy-interstitial pairs. In both cases the motion essentially occurs in a linear fashion for Au, while for Ag a more cooperative process is involved resulting in a reoriented split interstitial.

C_{60} again behaves differently from both Ag and Au. Here we found a simple migration mechanism for an O_h interstitial along a $\langle 100 \rangle$ direction through a $\langle 100 \rangle$ -split-interstitial transition state (Fig. 15). Since the SC Au potential has a shorter effective range than that for Ag, while the effective range of the Girifalco C_{60} potential is shorter still, it appears that $\langle 100 \rangle$ split interstitials are favorable for longer-ranged potentials and O_h interstitials are unfavorable, while the converse holds for shorter-ranged potentials. The energetics of these rearrangements are summarized in Table VIII.

The possibility of a $\langle 110 \rangle$ split interstitial was also investigated. A low-index stationary point for C_{60} was not found, but for SC Ag and Au the configuration corresponds to a transition state for a 90° rotation of the $\langle 100 \rangle$ split interstitial. The defect does not actually migrate in this process (Fig. 16); details of the pathways are given in Table IX. Analogous rotation of $\langle 110 \rangle$ dumbbells has previously been proposed to explain the relaxation of radiation-induced point defects in body-centered-cubic Mo (Ref. 67) and W.⁶⁸ However, alternative mechanisms have also been suggested.⁶⁹ The fact that Ag favors $\langle 100 \rangle$ over $\langle 110 \rangle$ split interstitials with the present potential is in agreement with experiment.⁷⁰

The barriers involved for the $\langle 100 \rangle$ -split-interstitial rotation are clearly much larger than for the migration processes in Table VIII, which are themselves orders of magnitude smaller (for Ag and Au) than for any of the vacancy migrations reported in the previous section. The values obtained for Au, in particular, are almost an order

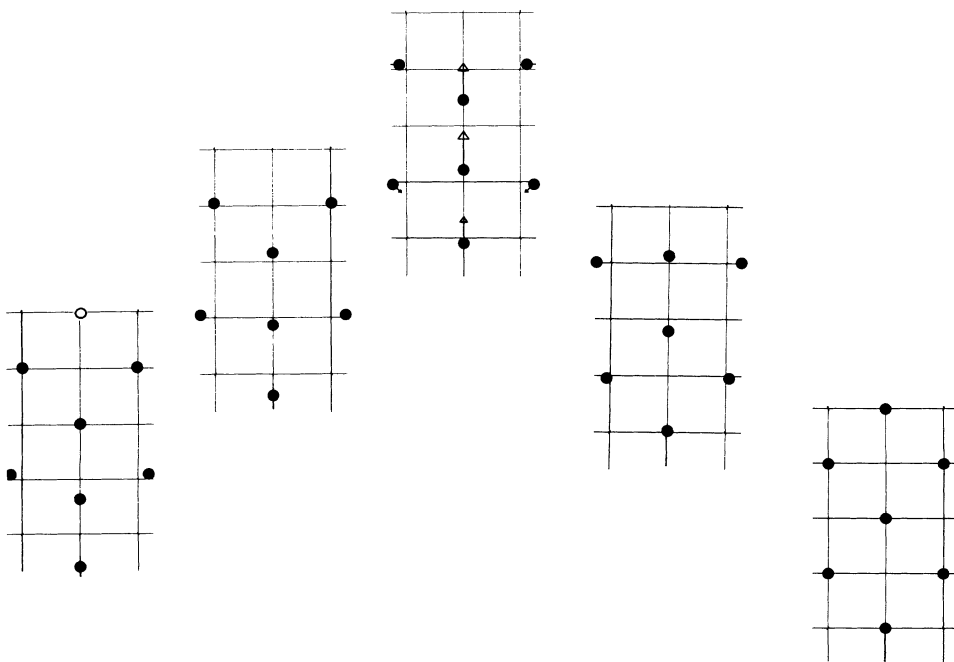


FIG. 10. Rearrangement of a $\langle 100 \rangle$ -split-interstitial/vacancy pair (left) to the fcc lattice (right) for SC Au viewed in a section of the (001) plane. The vacancy is marked with an open circle.

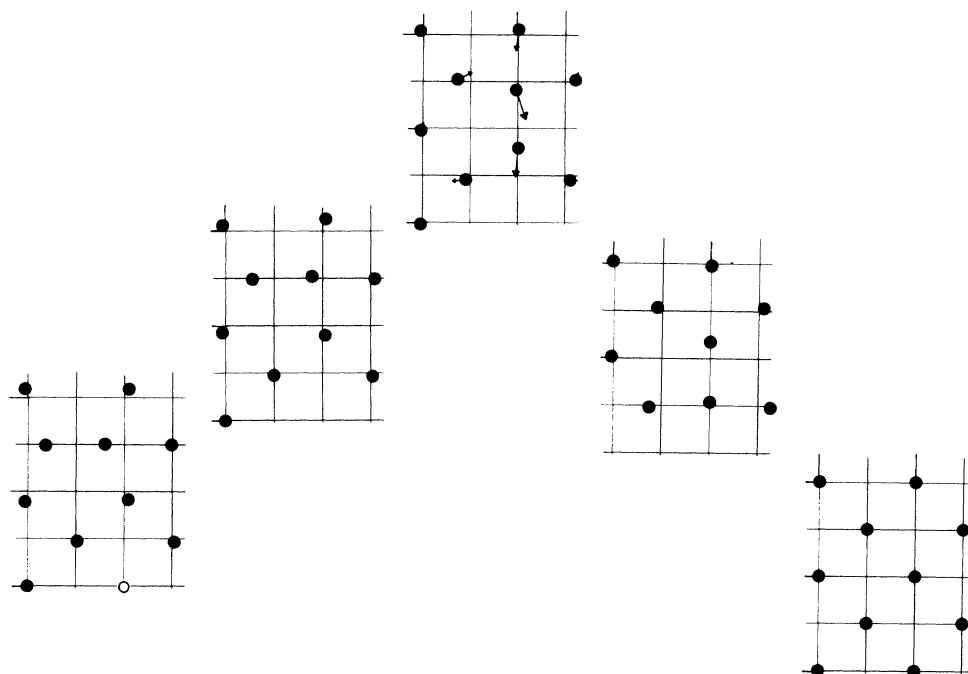


FIG. 11. Rearrangement of a $\langle 100 \rangle$ -split-interstitial/vacancy pair (left) to the fcc lattice (right) for SC Ag viewed in a section of the (001) plane. In this case the split interstitial lies perpendicular to the axis along which the three atoms appear to be moving in the transition state. The vacancy is marked with an open circle.

of magnitude smaller than for Ag. This is especially interesting in view of the anomalous migration observed in Au at very low temperatures, which Koehler has previously suggested is due to a $\langle 110 \rangle$ crowdion,⁷¹ i.e., an interstitial atom whose presence is "diluted" over a region of about eight interatomic distances.⁷² However, the larger formation energies of all the interstitials found in this study suggest that relatively high temperatures would be needed before thermally generated interstitials could contribute significantly to diffusion. When compared to divacancies the formation energies are greater

but the barriers are lower. The present results suggest that the divacancy mechanism has the lower sum of energies.

VIII. COOPERATIVE REARRANGEMENTS

A few highly cooperative processes were found for all three systems. In these mechanisms, which have extremely high barriers, essentially all the atoms or mole-

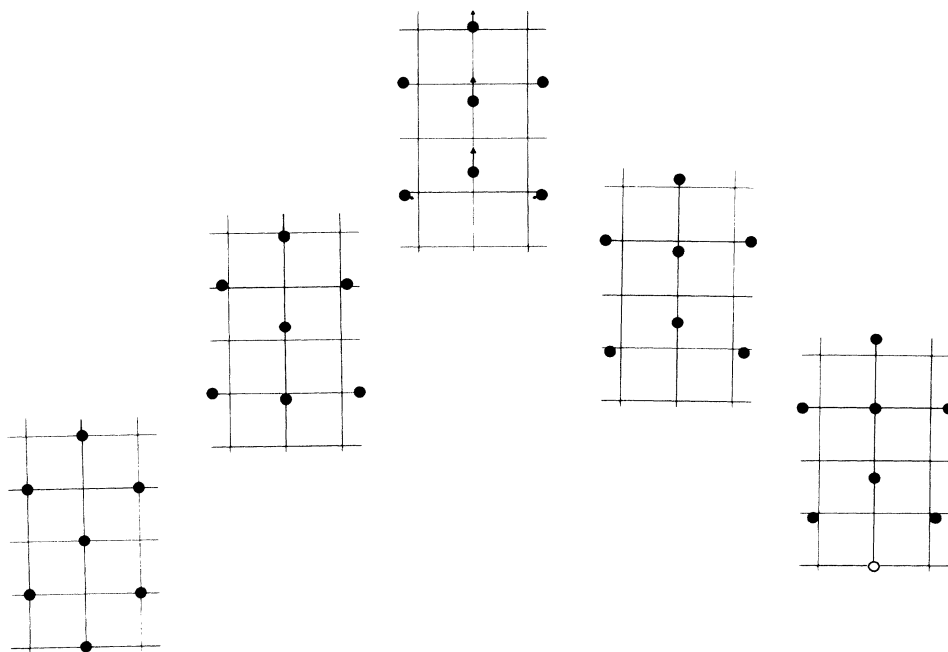


FIG. 12. Formation of an O_h -interstitial/vacancy pair (right) from the fcc lattice (left) for C_{60} viewed in a section of the (001) plane. The vacancy is marked by an open circle.

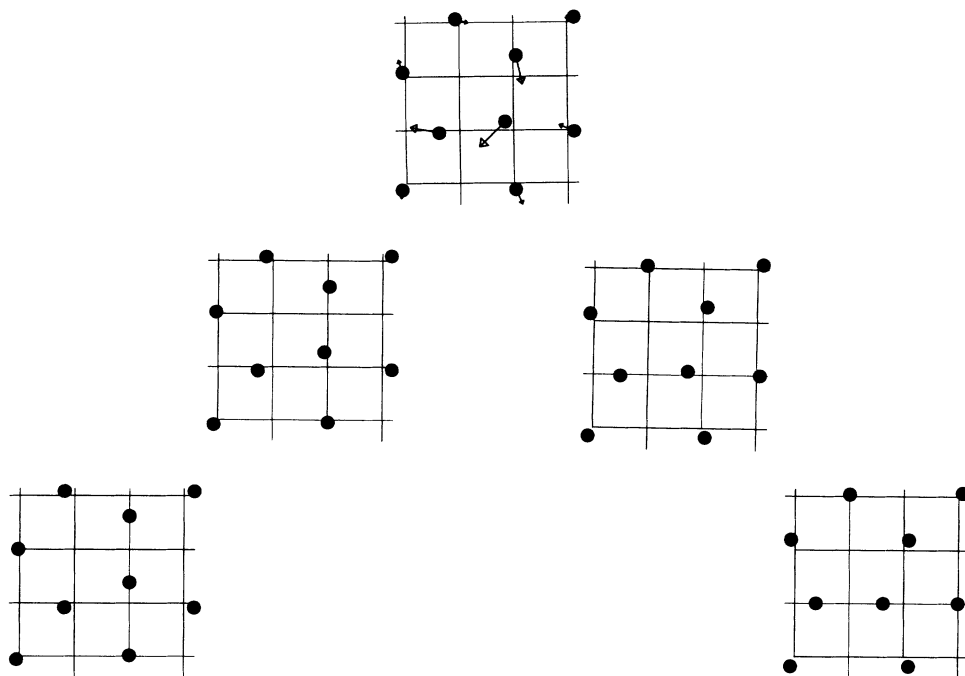


FIG. 13. Migration of the $\langle 100 \rangle$ -split-interstitial for Ag viewed in a section of the (001) plane.

cules move. If these motions were commensurate with the periodic boundary conditions then we could clearly dismiss them as artifacts of the model used to represent the extended system. However, this does not appear to be the case, and so it is possible that these rearrangements are telling us something about the preferred cooperative motions of the bulk. The results will be summarized briefly here, if only to show that such mechanisms exist for the conventional representation of extended systems.⁷³

The first fully cooperative process was found in a transition-state search for SC Ag and links the regular fcc lattice to a structure with no discernible order at all. The pathway is highly asymmetrical because the disordered minimum lies much higher in energy. An equivalent

pathway exists for Au, but when a transition-state search was performed for C_{60} starting from the rescaled geometry for Ag it took 88 cycles to converge. The resulting pathway appears to link two high-energy, disordered minima.

The second cooperative process is rather different. In this case the barriers are again large but the fcc lattice is connected to a new minimum with almost the same energy which possesses multiple twins on a set of $\{111\}$ planes. The symmetry inherent in this process only becomes apparent when the pathway is viewed down the $[1\bar{1}0]$, $[10\bar{1}]$, or $[01\bar{1}]$ directions. The same process occurs for all three potentials.

The final cooperative rearrangement was found initially in a transition-state search from the regular C_{60} lattice.

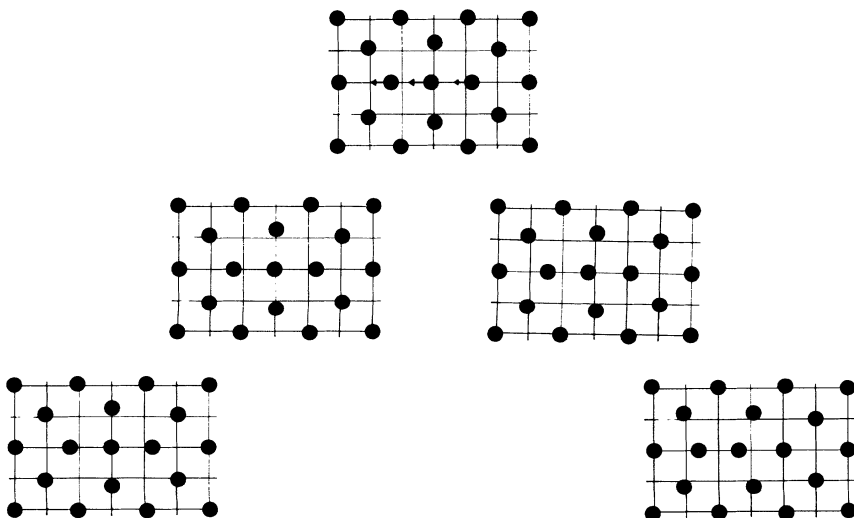


FIG. 14. Rearrangement from an O_h interstitial to a $\langle 100 \rangle$ split interstitial for Au viewed in a section of the (001) plane.

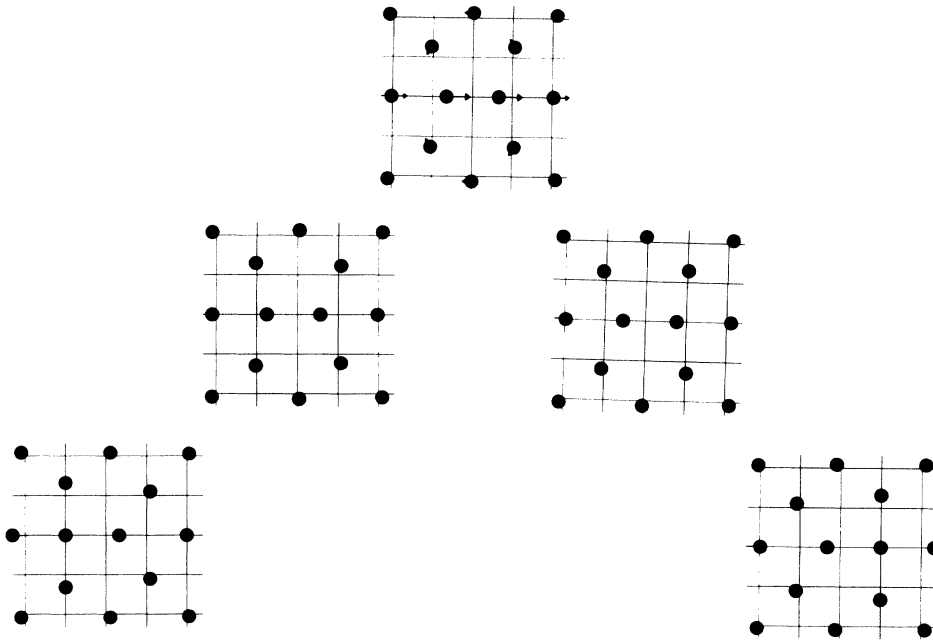


FIG. 15. Migration of an O_h interstitial via a $\langle 100 \rangle$ split interstitial transition state for C_{60} viewed in a section of the (001) plane.

Starting from the rescaled C_{60} transition state SC Ag converged to a transition state in 24 steps, and the two mechanisms are found to be very similar, with SC Au behaving in the same way as Ag. In all three cases the symmetry of the rearrangement becomes clear when the pathway is viewed down the $[110]$ direction, and is then seen to involve diamonds of 16 atoms or molecules. An alternative description of the intermediate geometries is that they possess stacking faults on inclined $\{111\}$ planes. However, particles also migrate between planes parallel to this direction. For C_{60} the diamonds undergo a slight relative rotation to give a high-energy minimum. However, for Ag and Au the diamonds do not “rock” when viewed in this direction but expand and contract slightly, and the regular fcc lattice is recovered.

IX. DIFFUSION CONSTANTS AND LATTICE RELAXATION

The phenomenological diffusion equation is

$$D = D^0 e^{-Q/kT}, \quad (10)$$

where D^0 is the diffusion constant and Q is the effective activation energy.⁶⁵ The transition-state-theory expression, due to Vineyard,¹² is

$$D = \frac{1}{6} a^2 f_{\text{fcc}} \left[\frac{\prod_{j=1}^{3N-3} \nu_j^{\min}}{\prod_{k=1}^{3N-4} \nu_k^{\text{TS}}} \right] e^{-\Delta E/kT}, \quad (11)$$

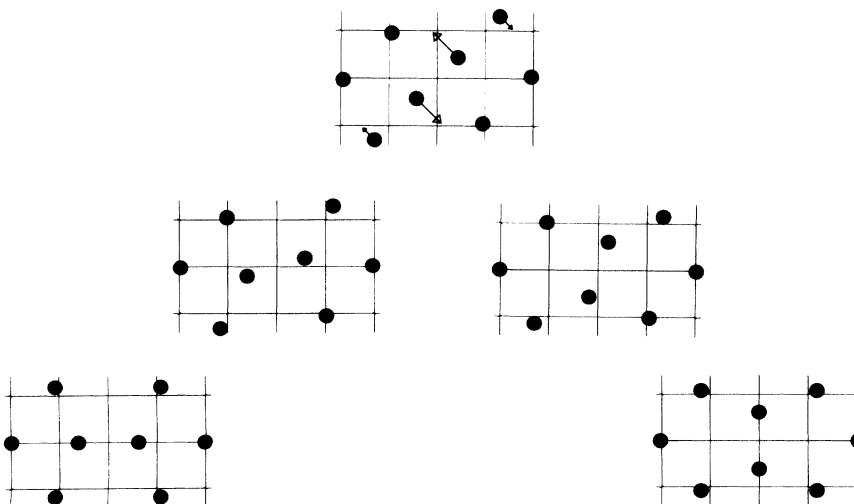


FIG. 16. Rotation of a $\langle 100 \rangle$ split interstitial via a $\langle 110 \rangle$ split interstitial transition state for SC Ag viewed in a section of the (001) plane.

TABLE VII. Rearrangement pathways for vacancy-interstitial formation from the regular fcc lattice for all three potentials. The unit of energy is eV for Ag and Au and the pair well depth for C_{60} . MIN1 and MIN2 are the two minima, Δ_1 and Δ_2 are the two barriers. S , D , and γ are defined in Sec. V and ω is the magnitude of the unique imaginary normal-mode frequency of the transition state in cm^{-1} .

MIN1	Δ_1	TS	Δ_2	MIN2	S (Å)	D (Å)	γ	ω
SC Ag								
vacancy- $\langle 100 \rangle$ -interstitial ^a	0.1250	-738.862 682	4.9059	fcc	8.01	4.76	111.1	19.2
SC Au								
vacancy- $\langle 100 \rangle$ -interstitial ^b	0.0214	-961.628 647	3.7887	fcc	7.37	5.29	107.9	12.3
C_{60}								
vacancy- O_h -interstitial ^c	7.8446	-1471.717 725	184.1249	fcc	23.66	15.88	89.0	14.4

^a $E = -738.987\,707$ eV.

^b $E = -961.650\,081$ eV.

^c $E = -1479.562\,331$ pair well depths.

TABLE VIII. Rearrangement pathways for interstitials in SC Ag, SC Au, and C_{60} ; in each case the cubic cell contains 257 atoms or molecules. The unit of energy is eV for Ag and Au and the pair well depth for C_{60} . MIN1 and MIN2 are the two minima, Δ_1 and Δ_2 are the two barriers. S , D , and γ are defined in Sec. V and ω is the magnitude of the unique imaginary normal-mode frequency of the transition state in cm^{-1} .

MIN1	Δ_1	TS	Δ_2	MIN2	S (Å)	D (Å)	γ	ω
SC Ag								
$\langle 100 \rangle$ interstitial ^a	0.0500	−742.830 490	0.0500	$\langle 100 \rangle$ interstitial	2.35	2.21	31.8	21.4
SC Au								
O_h interstitial ^b	0.0012	−966.075 706	0.0076	$\langle 100 \rangle$ interstitial ^c	1.48	1.44	33.7	3.4
C_{60}								
O_h interstitial ^d	9.6492	−1482.713 099	9.6492	O_h interstitial	13.02	10.82	22.4	11.8

^a $E = -742.880\,479$ eV.

^b $E = -966.076\,940$ eV.

^c $E = -966.083\,275$ eV.

^d $E = -1492.362\,298$ pair well depths.

TABLE IX. Pathways for the local rotation of $\langle 100 \rangle$ split interstitials in SC Ag and Au via a $\langle 110 \rangle$ split interstitial transition state. In each case the cubic cell contains 257 atoms and the unit of energy is eV. MIN1 and MIN2 are the two minima, Δ_1 and Δ_2 are the two barriers. S , D , and γ are defined in Sec. V and ω is the magnitude of the unique imaginary normal-mode frequency of the transition state in cm^{-1} .

MIN1	Δ_1	TS	Δ_2	MIN2	S (Å)	D (Å)	γ	ω
SC Ag								
$\langle 100 \rangle$ interstitial ^a	0.4200	−742.460 450	0.4200	$\langle 100 \rangle$ interstitial	4.75	3.07	60.9	42.2
SC Au								
$\langle 100 \rangle$ interstitial ^b	0.3005	−965.782 798	0.3005	$\langle 100 \rangle$ interstitial	5.03	3.03	63.7	28.0

^a $E = -742.880\,479$.

^b $E = -966.083\,275$.

where a is the nearest-neighbor distance, f_{fcc} is the correlation factor equal to 0.781 for nearest-neighbor vacancy migration⁶⁵ and 0.468 for divacancy migration,⁷⁴ ν_j^{min} and ν_k^{TS} are normal-mode frequencies of the minimum and transition state in question, and ΔE is the sum of the defect formation and migration energies. This expression assumes that we may neglect the entropy differences and the difference between enthalpies and internal energies.

In fact, one can equally well use a Rice-Ramsperger-Kassel-Marcus-type expression for the rate,⁸⁷ rather than transition-state theory, and it is not hard to show that the two become equal in the limit of high temperature. However, only the transition-state-theory values for D^0 will be given here.

Results will only be reported for the rearrangements which seem most likely to contribute to self-diffusion and

TABLE X. Collected data for key parameters calculated for SC Ag, SC Au, and C₆₀ in the present work (in bold), and comparison with experiment and previous calculations. All diffusion constants are in units of cm² s⁻¹ and energies are in eV in each case; corresponding results for Pt and Rh may be obtained by simply rescaling the SC results for Au and Ag, respectively. A superscript F signifies a formation energy calculated as described in Sec. V, and superscript M signifies a migration energy (barrier height). $Q = \Delta E^F + \Delta E^M$ is the effective activation energy for diffusion by a particular mechanism. Subscript $1v$ signifies single-vacancy properties, $2v$ signifies the 254D divacancy, "sec" signifies the second-nearest-neighbor vacancy migration, O_h signifies an octahedral interstitial, and $\langle 100 \rangle$ signifies a split interstitial. $\Delta E_{2v}^B = 2\Delta E_{1v}^F - \Delta E_{2v}^F$ is the divacancy binding energy. Overbars denote calculations in which the lattice was also relaxed.

Parameter	SC Ag	SC Au	C ₆₀
ΔE_{1v}^F	1.05, ^a 0.99, ^b 1.10, ^c 0.9, ^d 1.11, ^e 1.02, ^f 1.09 ^g 1.23, ^h 1.16, ⁱ 0.98 , 0.99	0.87, ^b 0.94, ^e 0.9, ^f 0.85, ^d 0.98, ^g 0.97, ⁱ 1.24, ^h 0.66 , 0.66	1.79, 1.80
ΔE_{1v}^M	0.64, ^c 0.8, ^f 0.65, ^e 0.73 , 0.73	0.85, ^f 0.84, ^e 0.57, 0.57	6.28, 6.01
Q_{1v}	1.96, ^j 1.99, ^l 1.79, ^m 1.91, ⁿ 1.82, ^f 1.76, ^e 1.92, ^g 1.76, ^c 2.06, ^h 1.71 , 1.72	1.75, ^f 1.78, ^e 1.83, ^k 1.81, ^g 2.07, ^h 1.23, 1.23	8.08, 7.81
D_{1v}^0	0.67, ^j 0.895, ^l 0.07, ^m 0.40, ⁿ 0.1, ^f 0.00011 , 0.0023	0.048, ^f 0.107, ^k 0.000040 , 0.0010	1.8×10^{-9} 1.5×10^6
ΔE_{sec}^M	3.17, 2.39	2.44, 1.83	32.16, 25.50
Q_{sec}	4.15, 3.38	3.10, 2.49	33.95, 27.30
ΔE_{2v}^F	1.88, 1.88	1.28, 1.27	3.34, 3.34
ΔE_{2v}^M	0.67, ^f 0.40 , 0.40	0.66, ^f 0.38, 0.38	2.66, 2.63 ^o
Q_{2v}	2.37, ^f 2.28 , 2.28	2.30, ^f 1.66 , 1.65	6.00, 5.97
D_{2v}^0/D_{1v}^0	55, ^f 37, 0.20	32, ^f 52, 1.32	
ΔE_{2v}^B	0.34, ^f 0.03, ^d 0.08 , 0.10	0.16, ^f -0.04, ^d 0.04 , 0.05	0.25, 0.26
$\Delta E_{\langle 100 \rangle}^F$	2.57, ^d 3.78 , 3.61	3.2, ^p 2.26, ^d 3.09 , 2.90	
$\Delta E_{\langle 100 \rangle}^M$	0.050 , 0.045	0.0076 , 0.0015	
$Q_{\langle 100 \rangle}$	3.83, 3.65	3.10, 2.90	
$\Delta E_{O_h}^F$	2.72 ^d	2.29, ^d 3.10, 2.90	46.94, 33.46
$\Delta E_{O_h}^M$		0.0012 , 0.0033	2.68, 1.44
Q_{O_h}		3.10, 2.90	49.62, 34.90

^aReference 77.

^bReference 78.

^cReference 79.

^dReference 14.

^eReference 8.

^fReference 80.

^gReference 81.

^hReference 34.

ⁱReference 82.

^jReference 83.

^kReference 84.

^lReference 85.

^mReference 74.

ⁿReference 86.

^oThese numbers are for the larger barrier; the smaller one (0.14 eV) is practically unchanged by relaxation.

^pReference 65.

are collected in Table X along with some experimental and theoretical values from the literature. The agreement obtained is quite encouraging, especially for Ag. In making such comparisons, however, we must be aware that all the results reported here so far are for constant-volume rather than constant-pressure calculations. Hence some selected stationary points were reoptimized with respect to the box length L while keeping the ratio of the cutoff to the box length fixed. Effective pressures were also calculated for all the stationary points, using

$$P = - \frac{dE}{dL} \frac{1}{3L^2} . \quad (12)$$

These required numerical derivatives of the total energy with respect to the box length, which were found from two-sided differences. In fact, because of the cutoff and minimum-image convention one must be especially careful in employing numerical derivatives. There is also the question of whether the cutoff should be incremented with the box length when the numerical derivatives are being calculated, or once the optimum value of L has been found. (This should not affect the final optimized geometry.) The most stable scheme consisted of incrementing the cutoff in proportion to the box length with displacements of around 10^{-6} Å. To optimize the box length a simple golden section search method was employed for SC potentials⁷⁵ and numerical first and second derivatives were used in a one-dimensional eigenvector-following scheme for C_{60} . For all three systems lattice-optimization steps alternated with standard eigenvector-following steps for the positions of the particles within the box. This procedure generally converged more slowly for C_{60} .

The results for the unrelaxed stationary points show the following features.

- (i) All Ag and Au defect minima have $P \sim -10^3$ atm.
- (ii) Ag and Au fcc lattices have $P = -0.4$ and 200 atm, respectively.
- (iii) C_{60} vacancy minima have $P \sim -1$ atm; the fcc lattice has $P = 1.3$ atm.
- (iv) Divacancy transition states have $P \sim \pm 10^2$ atm, the plus for Ag and Au and the minus for C_{60} .
- (v) The single-vacancy transition state has $P \sim 10^2, 10^3$, and -10^2 atm for Ag, C_{60} , and Au, respectively.
- (vi) Trivacancy transition states have $P \sim \pm 10^3$ atm, the minus for Ag and Au, and the plus for C_{60} , except that the C_{60} transition state leading to a minimum with an off-site molecule has $P = -10$ atm.
- (vii) All stationary points calculated for cells containing 257 particles have $P \sim 10^5$ atm, as do the transition states corresponding to cooperative rearrangements.

Transition states for C_{60} generally have positive pressures, even when there are several vacancies present. This presumably again reflects the short range of the C_{60} potential: the relatively narrow width of the potential well means that favorable interactions in an ordered local minimum rapidly become unfavorable when some distances are shortened in a transition-state geometry. In general, the pressure is always less than 1 atm in magnitude after the box size has been optimized.

In agreement with the above observations, the results

for C_{60} are significantly more sensitive to lattice relaxation than those for Ag and Au. Considering first the vacancy and divacancy mechanisms, the formation energies for Ag and Au are hardly affected by relaxation, and migration energies only decrease by a few percent. The diffusion constants, however, are much more sensitive because the products of normal-mode frequencies can change significantly. For Ag and Au D_{1v}^0 increases on relaxation, moving closer to experiment, but the ratio D_{2v}^0/D_{1v}^0 agrees less well with experiment after relaxation.

For C_{60} the changes are more pronounced. The spectacular increase in D_{1v}^0 on relaxation occurs because all the normal-mode frequencies of the transition state decrease by a couple of wave numbers on relaxation, whereas those of the corresponding minimum fall only slightly. Hence the diffusion constants are likely to be the least trustworthy of the numerical results reported; nevertheless, studies of the pressure dependence of diffusion and other properties of C_{60} might be worthwhile.

For mechanisms involving interstitials the effects of relaxation are more noticeable for Ag and Au, and are significant for the C_{60} O_h interstitial. In all cases relaxation lowers the defect formation energy, and usually the migration energy decreases too, indicating that transition states generally relax more than minima, as expected and in agreement with previous work.³⁴ The significantly larger formation energy of interstitials compared to vacancies and divacancies contrasts with the predictions of Flores and March⁷⁶ for Na and K.

X. CONCLUSIONS

The most important conclusion is that eigenvector following can locate transition states for extended systems and, perhaps for the first time, has given detailed insight into rearrangement mechanisms. The scope for future studies of both bulk and surfaces is limited principally by the availability of realistic empirical potentials or efficient *ab initio* energy derivatives.

The two principal weaknesses of the present work are the size of the cubic cell used to represent the bulk and the empirical potentials employed. Fuks *et al.*¹⁰ have previously criticized calculations in which cells containing only around 100 atoms are used, since the effective defect concentration is then several orders of magnitude higher than in the solid at the melting point. There is some evidence in the present work, from the formation energies of well-separated divacancies, that this is not a problem here. However, further investigation will be needed in the future employing a larger cubic cell to discover how well the results are converged with respect to the cell size. The boundary conditions will probably affect delocalized mechanisms the most, and this is a particular concern for the highly cooperative processes discussed in Sec. VIII. It is not clear from this initial study whether the latter contain any useful information or are merely artifacts.

There is one further potential source of difficulties in comparing the present results with experiment, namely, that the calculations are all of internal energies rather

than enthalpies, and that entropy has been neglected. However, the comparisons between constant-volume and constant-(zero-) pressure results, the latter corresponding to fully relaxed lattices, should provide a good indication of the importance of such effects.

The much shorter effective range of the C_{60} potential produces several predictions which are qualitatively different from the Sutton-Chen Ag and Au potentials. Examples are C_{60} minima with off-site molecules and the calculated pressures and relaxation effects for C_{60} . It also appears that $\langle 100 \rangle$ split interstitials are favorable for systems bound by longer-range potentials, and O_h interstitials are unfavorable, whilst the converse holds for systems bound by short-range potentials. For Au these two defects have very similar energies. A general feature of the results for all three potentials is that formation of multiple vacancies is most favorable when they lie at nearest-neighbor sites, as expected.

Divacancy migration has the lowest combined formation and migration energy aside from the monovacancy mechanism. Furthermore, the relatively small effect of lattice relaxation upon the energetics for Ag and Au suggests that a second mechanism is more likely to be the cause of the upward curvature of Arrhenius plots at high temperature than temperature dependence of the formation and migration energies. Of course, this assumes that the principal effect of temperature variation would be similar to relaxation. For all three potentials the second-nearest-neighbor migration is predicted to be more favorable energetically than mechanisms involving interstitials. Divacancy and trivacancy migration mechanisms

with particularly low barriers occur for all three potentials when the vacancies are adjacent. In such cases the energy of the transition state is lowered by deviation of the migrating atom towards spectator vacancies, thereby increasing the number of favorable interactions.

Some differences have also been observed between the Sutton-Chen Ag and Au potentials. For Au direct motion in which three atoms move in a $\langle 100 \rangle$ direction is favored over the more cooperative processes which are found in Ag. However, it is not obvious how this observation is related to the results for migration on (100) surfaces.¹⁸ The somewhat better agreement with experiment obtained for most properties with the Ag potential may be a further indication that the SC Ag potential is a better representation of Ag than the SC Au potential is of Au. This has previously been suggested on the basis of calculations for small clusters.¹⁹

Finally, the present study raises the important question of how worthwhile an "accurate" quantum-mechanical calculation is without proper geometry optimization, and, conversely, how worthwhile accurate geometry optimization is for simple empirical potentials.

ACKNOWLEDGMENTS

We thank Professor C. R. A. Catlow for drawing our attention to previous work on ionic systems, and Professor A. E. DePristo, Professor L. Girifalco, Dr. R. M. Lynden-Bell, and Dr. A. P. Sutton for helpful discussions. D.J.W. thanks the Royal Society and the SERC for their support.

*Present address: Biomolecular Structure and Modelling Unit, Department of Biochemistry, University College London, Gower Street, London WC1E 6BT.

¹A. P. Sutton and J. Chen, *Philos. Mag. Lett.* **61**, 139 (1990).

²L. A. Girifalco, *J. Phys. Chem.* **96**, 858 (1992).

³H. B. Huntington and F. Seitz, *Phys. Rev. B* **61**, 315 (1942); H. B. Huntington, *ibid.* **61**, 325 (1942).

⁴A. G. Mikhin and T. N. Osetsky, *J. Phys. Condens. Matter* **5**, 9121 (1993).

⁵D. H. Tsai, R. Bullough, and R. C. Perrin, *J. Phys. C* **3**, 2022 (1970).

⁶G. Neumann, C. Tuijn, G. De Vries, and H. Bakker, *Phys. Status Solidi B* **149**, 483 (1988).

⁷W. Frank, in *Point Defects and Defect Interactions in Metals*, edited by J.-I. Takamura, M. Doyama, and M. Kiritani (North-Holland, Amsterdam, 1982), p. 203.

⁸R. W. Siegel, in *Point Defects and Defect Interactions in Metals* (Ref. 7), p. 533.

⁹W. Schüle, in *Point Defects and Defect Interactions in Metals* (Ref. 7), pp. 209, 551.

¹⁰D. Fuks, J. Pelleg, S. N. Rashkeev, and S. Dorfman, *Z. Phys. B* **469**, 473 (1993).

¹¹G. L. Buchbinder, *Phys. Status Solidi B* **167**, 19 (1991).

¹²G. H. Vineyard, *J. Phys. Chem. Solids* **3**, 121 (1957).

¹³M. W. Finnis and J. E. Sinclair, *Philos. Mag. A* **50**, 45 (1984).

¹⁴R. Bauer, W. Maysenhölder, and A. Seeger, *Phys. Lett. A* **90**, 55 (1982).

¹⁵J. Uppenbrink, R. L. Johnston, and J. N. Murrell, *Surf. Sci.* **304**, 223 (1994).

¹⁶M. S. Daw and M. I. Baskes, *Phys. Rev. B* **29**, 1285 (1984).

¹⁷L. Marville and W. Andreoni, *J. Phys. Chem.* **91**, 2645 (1987).

¹⁸R. M. Lynden-Bell, *Surf. Sci.* **259**, 129 (1991).

¹⁹J. Uppenbrink and D. J. Wales, *J. Chem. Phys.* **98**, 5720 (1993).

²⁰M. H. J. Hagen, E. J. Meijer, G. C. A. M. Mooij, D. Frenkel, and H. N. W. Lekkerkerker, *Nature* **365**, 425 (1993).

²¹A. Cheng, M. L. Klein, and C. Caccamo, *Phys. Rev. Lett.* **71**, 1200 (1993).

²²N. W. Ashcroft, *Nature* **365**, 387 (1993).

²³P. A. Braier, R. S. Berry, and D. J. Wales, *J. Chem. Phys.* **93**, 8745 (1990).

²⁴F. H. Stillinger and D. K. Stillinger, *J. Chem. Phys.* **93**, 6106 (1990); J. Rose and R. S. Berry, *ibid.* **98**, 3262 (1993).

²⁵(a) D. J. Wales, *J. Chem. Soc. Faraday Trans.* **90**, 1061 (1994); (b) C. Rey, L. J. Gallego, and J. A. Alonso, *Phys. Rev. B* **49**, 8491 (1984); (c) D. J. Wales, *J. Chem. Phys.* **101**, 3570 (1994).

²⁶M. Allen and D. J. Tildesley, *The Computer Simulation of Liquids* (Clarendon, Oxford, 1987).

²⁷G. De Lorenzi, G. Jacucci, and C. P. Flynn, *Phys. Rev. B* **36**, 9461 (1987).

²⁸J. N. Murrell and K. J. Laidler, *J. Chem. Soc. Faraday Trans.* **2** **64**, 371 (1968).

²⁹J. Pancik, *Collect. Czech. Chem. Commun.* **40**, 1112 (1974); C. J. Cerjan and W. H. Miller, *J. Chem. Phys.* **75**, 2800 (1981).

³⁰J. Simons, P. Jørgenson, H. Taylor, and J. Ozment, *J. Phys. Chem.* **87**, 2745 (1983); D. O'Neal, H. Taylor, and J. Simons, *ibid.* **88**, 1510 (1984); A. Banerjee, N. Adams, J. Simons, and R. Shepard, *ibid.* **89**, 52 (1985).

- ³¹J. Baker, *J. Comput. Chem.* **7**, 385 (1986); **8**, 563 (1987).
- ³²A. R. DuCharme and H. T. Weaver, *Phys. Rev. B* **5**, 330 (1972).
- ³³G. De Lorenzi and F. Ercolessi, *Europhys. Lett.* **20**, 349 (1992).
- ³⁴A. Ghorai, *Phys. Rev. B* **46**, 5229 (1992).
- ³⁵A. De Vita and M. J. Gillan, *J. Phys. Condens. Matter* **3**, 6225 (1991).
- ³⁶P. J. H. Denteneer and J. M. Soler, *J. Phys. Condens. Matter* **3**, 8777 (1991).
- ³⁷G. De Lorenzi, C. P. Flynn, and G. Jacucci, *Phys. Rev. B* **30**, 5430 (1984).
- ³⁸B. Chakraborty and R. W. Siegel, in *Point Defects and Defect Interactions in Metals* (Ref. 7), p. 93.
- ³⁹O. Takai, M. Doyama, and Y. Hisamatsu, in *Point Defects and Defect Interactions in Metals* (Ref. 7), pp. 109, 113.
- ⁴⁰K. Masuda, in *Point Defects and Defect Interactions in Metals* (Ref. 7), p. 105.
- ⁴¹O. Takai, M. Doyama, and Y. Hisamatsu, in *Defects and Defect Interactions in Metals* (Ref. 7), p. 117.
- ⁴²N. V. Doan, in *Point Defects and Defect Interactions in Metals* (Ref. 7), p. 722.
- ⁴³N. F. Mott and M. J. Littleton, *Trans. Faraday Soc.* **34**, 485 (1938).
- ⁴⁴C. R. A. Catlow, *J. Chem. Soc. Faraday Trans. 2* **85**, 335 (1989).
- ⁴⁵A. B. Lidiard, *J. Chem. Soc. Faraday Trans. 2* **85**, 341 (1989).
- ⁴⁶J. H. Harding, *J. Chem. Soc. Faraday Trans. 2* **85**, 351 (1989).
- ⁴⁷M. Leslie, *J. Chem. Soc. Faraday Trans. 2* **85**, 407 (1989).
- ⁴⁸P. W. M. Jacobs, *J. Chem. Soc. Faraday Trans. 2* **85**, 415 (1989).
- ⁴⁹J. Corish, *J. Chem. Soc. Faraday Trans. 2* **85**, 437 (1989).
- ⁵⁰M. Marchese, G. Jacucci, and C. P. Flynn, *Phys. Rev. B* **36**, 9469 (1987).
- ⁵¹J. Viñals and R. F. Sekera, *Phys. Rev. B* **37**, 10 697 (1988).
- ⁵²J. Uppenbrink and D. J. Wales, *Chem. Phys. Lett.* **190**, 447 (1992).
- ⁵³L. S. Perkins and A. E. DePristo, *Surf. Sci.* **294**, 67 (1993); and (unpublished).
- ⁵⁴A. Ulitsky and R. Elber, *J. Chem. Phys.* **92**, 1510 (1990).
- ⁵⁵D. J. Wales, *J. Chem. Soc. Faraday Trans.* **86**, 3505 (1990).
- ⁵⁶D. J. Wales, *Mol. Phys.* **74**, 1 (1991).
- ⁵⁷(a) D. J. Wales, *J. Chem. Soc. Faraday Trans.* **88**, 653 (1992); (b) **89**, 1305 (1993).
- ⁵⁸E. B. Wilson, J. C. Decius, and P. C. Cross, *Molecular Vibrations* (Dover, New York, 1980).
- ⁵⁹In the current treatment the frequencies are calculated from the Hessian for the N atoms in the cubic cell but taking into account the periodic boundary conditions. In effect, the cubic cell can be considered as a "supermolecule" which is repeated over a simple cubic lattice. The normal-mode analysis for a single cell then gives $3N-3$ nonzero and three zero frequencies which correspond to the optical and acoustic modes of the lattice evaluated at wave vector $\mathbf{k}=0$.
- ⁶⁰H. Tanaka and I. Ohmine, *J. Chem. Phys.* **91**, 6318 (1989); I. Ohmine and H. Tanaka, *ibid.* **93**, 8138 (1990).
- ⁶¹F. H. Stillinger and T. A. Weber, *Phys. Rev. A* **23**, 2408 (1983).
- ⁶²S. Wolfram, *Mathematica*, 2nd ed. (Addison-Wesley, Redwood City, 1991).
- ⁶³J. W. McIver and R. E. Stanton, *J. Am. Chem. Soc.* **94**, 8618 (1972); R. E. Stanton and J. W. McIver, *ibid.* **97**, 3632 (1975).
- ⁶⁴F. Ercolessi, E. Tosatti, and M. Parrinello, *Phys. Rev. Lett.* **57**, 719 (1986); *Philos. Mag. A* **58**, 213 (1988).
- ⁶⁵See, e.g., R. J. Borg and G. J. Dienes, *Solid State Diffusion* (Academic, New York, 1988).
- ⁶⁶J. L. Bocquet, in *Point Defects and Defect Interactions in Metals* (Ref. 7), p. 664.
- ⁶⁷B. Beuneu and Y. Quéré, in *Point Defects and Defect Interactions in Metals* (Ref. 7), p. 156.
- ⁶⁸H. Mizubayashi, S. Okuda, and T. Arai, in *Point Defects and Defect Interactions in Metals* (Ref. 7), p. 167.
- ⁶⁹H. Jacques and K. H. Robrock, in *Point Defects and Defect Interactions in Metals* (Ref. 7), p. 159.
- ⁷⁰S. Okuda and H. Mizubayashi, in *Point Defects and Defect Interactions in Metals* (Ref. 7), p. 163.
- ⁷¹J. S. Koehler, in *Point Defects and Defect Interactions in Metals* (Ref. 7), p. 143.
- ⁷²H. R. Paneth, *Phys. Rev.* **80**, 708 (1950).
- ⁷³The authors are indebted to Dr. A. P. Sutton for his attempts to provide helpful descriptions of these processes.
- ⁷⁴H. Mehrer and F. Hutter, in *Point Defects and Defect Interactions in Metals* (Ref. 7), p. 558.
- ⁷⁵W. H. Press, B. P. Flannery, S. A. Teukolsky, and W. T. Vetterling, *Numerical Recipes* (Cambridge University Press, Cambridge, 1990).
- ⁷⁶F. Flores and N. H. March, in *Point Defects and Defect Interactions in Metals* (Ref. 7), p. 85.
- ⁷⁷K. Mosig, J. Wolff, J.-E. Kluin, and Th. Hehenkamp, *J. Phys. Condens. Matter* **4**, 1447 (1992).
- ⁷⁸A. D. Franklin, in *Point Defects in Solids*, edited by J. H. Crawford and L. M. Slifkin (Plenum, New York, 1972), Chap. 9, p. 27.
- ⁷⁹J. Hillairet, C. Mairy, C. Minier, P. Hautojärvi, A. Vehanen, and J. Yli-Kauppila in *Point Defects and Defect Interactions in Metals* (Ref. 7), p. 284.
- ⁸⁰W. Schüle and R. Scholz, in *Point Defects and Defect Interactions in Metals* (Ref. 7), p. 257.
- ⁸¹M. Doyama and J. S. Koehler, *Acta Metall.* **24**, 871 (1976).
- ⁸²L. Kornblit, *Phys. Status Solidi B* **115**, 485 (1983).
- ⁸³S. J. Rothman, N. L. Peterson, and J. T. Robinson, *Phys. Status Solidi* **39**, 635 (1970).
- ⁸⁴H. M. Gilder and D. Lazarus, *J. Phys. Chem. Solids* **26**, 2081 (1965).
- ⁸⁵W. A. Johnson, *Trans. Am. Inst. Min. Metall. Eng.* **143**, 107 (1941).
- ⁸⁶C. Kittel, *Introduction to Solid State Physics* 5th ed. (Wiley, New York, 1976), p. 543.
- ⁸⁷See, e.g., K. J. Laidler, *Chemical Kinetics*, 3rd ed. (Harper and Row, New York, 1987).